Response of Freshwater Flux and Sea Surface Salinity to Variability of the Atlantic Warm Pool

Chunzai Wang [1]

Liping Zhang [2, 1 & 3]

Sang-Ki Lee [2 & 1]

[1] NOAA Atlantic Oceanographic and Meteorological Laboratory

Miami, Florida

[2] Cooperative Institute for Marine and Atmospheric Studies
University of Miami
Miami, Florida

[3] Physical Oceanography Laboratory
Ocean University of China

Qingdao, China

Revised to *Journal of Climate*

August 2012

Corresponding author address: Dr. Chunzai Wang, NOAA/Atlantic Oceanographic and Meteorological Laboratory, 4301 Rickenbacker Causeway, Miami, FL 33149.
E-mail: Chunzai.Wang@noaa.gov.

Abstract

The response of freshwater flux and sea surface salinity (SSS) to the Atlantic Warm Pool (AWP) variations from seasonal to multidecadal timescales is investigated by using various reanalysis products and observations. All of data sets show a consistent response for all timescales: A large (small) AWP is associated with a local freshwater gain (loss) to the ocean, less (more) moisture transport across Central America and a local low (high) SSS. Our moisture budget analysis demonstrates that the freshwater change is dominated by the atmospheric mean circulation dynamics, while the effect of thermodynamics is of secondary importance. Further decomposition points out that the contribution of the mean circulation dynamics primarily arises from its divergent part which mainly reflects the wind divergent change in the low level as a result of SST change. In association with a large (small) AWP, warmer (colder) than normal SST over the tropical North Atlantic can induce anomalous low-level convergence (divergence), which favors anomalous ascent (decent) and thus generates more (less) precipitation. On the other hand, a large (small) AWP weakens (strengthens) the trade wind and its associated westward moisture transport to the eastern North Pacific across Central America, which also favors more (less) moisture resided in the Atlantic and hence more (less) precipitation. The results imply that variability of freshwater and ocean salinity associated with the AWP may have the potential to affect the Atlantic meridional overturning circulation.

1. Introduction

The Atlantic Warm Pool (AWP), defined by the sea surface temperature (SST) warmer than 28.5°C (Wang and Enfield 2001), is comprised of the Intra-America Seas (IAS) (i.e., the Gulf of Mexico and the Caribbean) and the western tropical North Atlantic (TNA). Unlike the Indo-Pacific warm pool, which straddles the equator, the AWP is entirely north of the equator and is sandwiched between the North and South Americas and between the tropical North Pacific and Atlantic Oceans. The AWP has a large seasonal cycle. In addition to the large seasonal cycle, the AWP shows variability on both interannual and multidecadal timescales as well as a long-term warming trend (Wang et al. 2008a), with large AWPs being almost three times larger than small ones (Wang and Enfield 2003).

Wang et al. (2006) demonstrated that summer rainfall in the Caribbean, Mexico and the eastern subtropical Atlantic is largely associated with the AWP variability by using a blend of satellite estimates and rain gauge data. Based on the NCAR atmospheric model, Wang et al. (2007, 2008b) further showed that the variability of AWP not only modulate local precipitation but also affect moisture export across Central America to the eastern North Pacific. A large (small) AWP can induce an anomalous ascent (decent) flow and thus leads to a significant response of an increased (a decreased) rainfall in the AWP region. Meanwhile, a large (small) AWP weakens (strengthens) the summertime Caribbean Low-Level Jet (CLLJ) (Wang 2007; Wang and Lee 2007) and the associated westward moisture transport, which is also in favor of generating an increased (a decreased) precipitation in the TNA.

However, how evaporation, precipitation, moisture transport and salinity vary with the

AWP is poorly known and understood, particularly in long-term observations. The freshwater variation can lead to a salinification or freshening of the subtropical North Atlantic Ocean, which is subsequently carried by the wind-driven ocean circulation (Thorpe et al. 2001; Vellinga and Wu 2004; Yin et al. 2006; Krebs and Timmermann 2007) to high latitudes where water cools and sinks. In this way, net freshwater flux and its corresponding salinity change over the AWP may have the potential to affect the deep water formation and the Atlantic meridional overturning circulation (Zaucker and Broecker 1992; Broecher 1997; Romanova et al. 2004). The purpose of the present paper is to present a quantitative evaluation of the net freshwater flux changes in response to the AWP variation. Since the local salinity response is not only determined by precipitation but also by evaporation, we thus assess the net freshwater flux of Evaporation minus Precipitation (EmP) associated with the AWP variability. Using several reanalysis products and observations, we examine the physical mechanisms of the net freshwater change associated with the AWP variation on various timescales. Additionally, we also give a quantitative evaluation of the moisture transport across Central America from the Atlantic to the Pacific associated with the AWP variability.

The paper is organized as follows. In the following section, we describe the data sets and methods that are used in this study. Section 3 shows the seasonal cycle of the freshwater flux, associated physical mechanisms, moisture transport, and sea surface salinity (SSS) in the AWP region. Sections 4 and 5 document these variations on interannual and multidecadal timescales, respectively. Finally, section 6 gives a summary and discussion.

2. Data sets and methodology

a. Data sets

Several atmospheric reanalysis data sets are used in this study. The first one is the National Centers for Environmental Prediction-National Center for Atmospheric Research (NCEP-NCAR) reanalysis field on a 2.5°×2.5° latitude-longitude horizontal grid (Kalnay et al. 1996). The data consist of daily fields from 1948 to 2010. The second data set is from the European Center for Medium Range Weather Forecast (ERA40) (Gibson et al. 1997), which spans from 1958 to 2001 and also has a horizontal resolution of 2.5°×2.5°. Another data set is the 20th Century Reanalysis version 2 (20CRv2), which contains the estimate of global tropospheric variability spanning from 1871 to 2010 at 6-hourly interval and with a spatial resolution of 2°×2° (Compo et al. 2011). In addition, the global ocean-atmosphere flux (OAFlux) product (Yu and Weller 2007) is also used to examine the evaporation change associated with the AWP. We also use the Global Precipitation Climatology Project (GPCP) (Adler et al. 2003) that is similar to the CPC (Climate Prediction Center) Merged Analysis of Precipitation (CMAP) (Xie and Arkin 1997). The GPCP data set blends satellite estimates and rain gauge data on a 2.5°×2.5° grid from January 1979 to 2010.

Three ocean reanalysis products are also used in this study: the Simple Ocean Data Assimilation (SODA) (Carton and Giese 2008), the German Estimating the Circulation and Climate of the Ocean (GECCO) (Kõhl et al. 2006), and the Geophysical Fluid Dynamics Laboratory (GFDL) (Rosati et al. 2004). The SODA uses an ocean general circulation model to assimilate available temperature and salinity observations. The product is a gridded data set of oceanic variables with monthly values and a 0.5°×0.5° horizontal resolution and 40 vertical levels. The version 2.2.4 of the SODA is used, with the time covering from 1871 to 2008. The GECCO is also a monthly product from 1952 to 2001, with a 1°×1° horizontal resolution and 23 vertical levels. The GFDL ocean product is from 1960 to 2004, with a 1°×1° resolution (enhanced to 1/3°×1/3° in the tropics between 30°S and 30°N) and 50 vertical levels. Additionally, the objectively analyzed temperature and salinity version 6.7 (Ishii et al. 2006) at 24 levels in the upper ocean of 1500 m from 1945-2010 is also used to study the salinity variability associated with the AWP variation. The analysis is based on the World Ocean Database/WOA05, the global temperature-salinity in the tropical Pacific from IRD/France, and the Centennial in situ Observation Based Estimates (COBE) sea surface temperature. The Ishii et al. analysis also includes the Argo profiling buoy data in the final several years and the XBT depth bias correction. Finally, we use the global gridded Argo data from Katsumata and Yoshinari (2010), which has a 1°×1° horizontal resolution and spans from 2001 to 2010.

b. Moisture budget

Following Peixoto and Oort (1992) and Trenberth and Guillemot (1995), we can write the vertically integrated moisture equation as:

$$(E-P)=\frac{\partial W}{\partial t}+\nabla\cdot(\frac{1}{g}\int_0^{p_s}[Uq]dp), \qquad (1)$$

where $W=(1/g)\int_0^{p_s}qdp$ is the column-integrated water vapor of the atmosphere; q, U, p_s, E and P are specific humidity, horizontal velocity, surface pressure, evaporation and precipitation, respectively. In this paper, $E-P$ is represented by EmP. The second integral on the right-hand side of Eq. (1) describes the divergence of water vapor horizontal flux. Integrating Eq. (1) over the globe, the divergence term becomes zero. Apparently, any variation in the global mean water vapor results from an imbalance between global-mean evaporation and precipitation. When time averages of Eq. (1) are taken for a month, the divergence of water vapor flux can be divided into the mean and transient eddy components in the form of

$$(\bar{E}-\bar{P})=\frac{\partial \bar{W}}{\partial t}+\nabla\cdot(\frac{1}{g}\int_0^{p_s}(\bar{U}\bar{q})\,dp)+\nabla\cdot(\frac{1}{g}\int_0^{p_s}(\overline{U'q'})dp)\equiv\frac{\partial \bar{W}}{\partial t}+DivQ_M+DivQ_E\,. \quad (2)$$

Overbar indicates monthly mean and prime represents departure from the monthly mean (by transient eddies). $DivQ_M$ represents the moisture flux divergence contributed from the mean (monthly to longer timescales) and $DivQ_E$ is the contribution from transient eddies (sub-monthly timescales). The water vapor flux divergence can be further broken up into the contributions that depend mostly on the mass divergence in the lower atmosphere and horizontal advection by the wind. Thus, Eq. (2) can be decomposed into

$$(\bar{E}-\bar{P})\approx\frac{\partial \bar{W}}{\partial t}+\frac{1}{g}\int_0^{p_s}(\bar{q}\nabla\cdot\bar{U})dp+\frac{1}{g}\int_0^{p_s}(\bar{U}\cdot\nabla\bar{q})dp+\frac{1}{g}\int_0^{p_s}\nabla\cdot(\overline{U'q'})dp\,. \quad (3)$$

Note that in Eq. (3) we have neglected the term of $(q_sU_s\cdot\nabla p_s)/g$ since this term (involved surface quantities) is very small based on our calculation [also see Seager and Naik (2010)].

We further examine the monthly change by denoting

$$\delta(\cdot)=(\cdot)-(\cdot)_C\,, \quad (4)$$

where $(\cdot)$ indicates each term of Eq. (3) at every month, and $(\cdot)_C$ indicates the long-term annual mean value. Then, Eq. (3) can be approximated as

$$\begin{aligned}\delta(\bar{E}-\bar{P})&\approx\delta(\frac{\partial \bar{W}}{\partial t})+\frac{1}{g}\int_0^{p_s}\delta(\bar{q}\nabla\cdot\bar{U})dp+\frac{1}{g}\int_0^{p_s}\delta(\bar{U}\cdot\nabla\bar{q})dp+\frac{1}{g}\int_0^{p_s}\nabla\cdot\delta(\overline{U'q'})dp\\&=\delta(\frac{\partial \bar{W}}{\partial t})+\frac{1}{g}\int_0^{p_s}(\delta\bar{q}\nabla\cdot\bar{U}_C+\bar{q}_C\nabla\cdot\delta\bar{U}+\delta\bar{U}\cdot\nabla\bar{q}_C+\bar{U}_C\cdot\nabla\delta\bar{q})dp+\frac{1}{g}\int_0^{p_s}\nabla\cdot\delta(\overline{U'q'})dp\end{aligned}\,. \quad (5)$$

Following Seager and Naik (2010), terms in Eq. (5) involving change in q but no change in U (i.e., U_C) are referred to as thermodynamic contributors to the change in column-integrated water vapor, and terms involving change in U but no change in q (i.e., q_C) are referred to as dynamic contributors. Note that the nonlinear term ($\int_o^{p_s} \nabla \cdot (\delta \bar{q}\, \delta \bar{U})\, dp$) that is the product of changes in both time mean specific humidity and flow is neglected because of its small magnitude. Briefly, the thermodynamic contributions are in the form of

$$\delta TH = \frac{1}{g}\int_0^{p_s} (\delta \bar{q} \nabla \cdot \bar{U}_C + \bar{U}_C \cdot \nabla \delta \bar{q})dp \equiv \delta TH_D + \delta TH_A, \quad (6)$$

and the dynamic contributions are

$$\delta MCD = \frac{1}{g}\int_0^{p_s} (\bar{q}_C \nabla \cdot \delta \bar{U} + \delta \bar{U} \cdot \nabla \bar{q}_C)dp \equiv \delta MCD_D + \delta MCD_A. \quad (7)$$

In Eqs. (6) and (7), we can further decompose the thermodynamic and dynamic contributions into terms due to the flow divergence (subscript D) and the advection of moisture (subscript A):

$$\delta TH_D = \frac{1}{g}\int_0^{p_s} (\delta \bar{q} \nabla \cdot \bar{U}_C)\, dp, \quad (8)$$

$$\delta TH_A = \frac{1}{g}\int_0^{p_s} (\bar{U}_C \cdot \nabla \delta \bar{q})\, dp, \quad (9)$$

$$\delta MCD_D = \frac{1}{g}\int_0^{p_s} (\bar{q}_C \nabla \cdot \delta \bar{U})\, dp, \quad (10)$$

$$\delta MCD_A = \frac{1}{g}\int_0^{p_s} (\delta \bar{U} \cdot \nabla \bar{q}_C)\, dp. \quad (11)$$

All terms in these equations are obtained with the originally daily or monthly data and then are averaged to climatological seasonal cycle and summer (fall) mean time series to focus on various timescale variations.

c. Moisture transport

Freshwater flux change over the AWP is influenced by or related to the moisture transport across the Americas from the Atlantic to the Pacific. To calculate moisture transport across the Americas, we use a method suggested by Richter and Xie (2010) who define 13 line segments (Fig. 1) that run approximately along the Atlantic drainage, integrate the moisture flux across each line segment and thus obtain the cross-isthmus moisture transport. The equation for an individual line segment is

$$\overline{MT} = \int_p \int_l (\overline{uq})\, dl \frac{dp}{g} = \int_p \int_l (\bar{u}\bar{q})\, dl \frac{dp}{g} + \int_p \int_l (\overline{u'q'})\, dl \frac{dp}{g} \equiv MT_M + MT_E, \qquad (12)$$

where *MT* is the moisture transport across the line segment, *p* is pressure, *l* is position along the segment, *q* is specific humidity and *g* is gravity. Overbar indicates monthly mean and prime indicates departure from the monthly mean. Thus, moisture transport can be decomposed into contributions by the mean (MT_M) and transient eddies (MT_E). Here we choose the integration from segments 6 to 10 (see Fig. 1), i.e., the moisture transport across Central America. A positive value of *MT* is indicative of a moisture export from the Atlantic to the Pacific basin and vice versa.

3. Annual variability

In this section, we first describe the EmP seasonal cycle in the AWP region. We then show physical processes that control the EmP seasonal cycle. The seasonality of the moisture transport across Central America and its relationship with the CLLJ are discussed in next sub-section. Finally, we examine the seasonal variability of sea surface salinity (SSS).

a. EmP seasonal cycle

To show the seasonal cycle of net freshwater flux over the AWP region, we calculate the EmP variation (climatology minus long-term mean) from January to December in the region of 5°N to 30°N from the American coast to 40°W based on various data sets (the left panels of Fig. 2). Note that evaporation in 20CRv2 and NCEP is computed from the model output of latent heat flux because of the lack of direct evaporation data. As shown in these panels, EmP is characterized by a significant annual cycle, with an excess of freshwater during May-November and a deficit of freshwater in the winter and early spring. The EmP seasonal cycle co-varies well with the variation of the AWP (Wang and Enfield 2003), in which the appearance (disappearance) of the AWP from May to November (December to April) (Fig. 2g) coincides with the excess (deficit) of precipitation. As shown in Fig. 2g, the AWP almost does not exist in the winter and spring if the AWP is defined by SST larger than 28.5°C. This implies that the AWP plays an important role in modulating local freshwater flux. A further analysis finds that the precipitation change dominates the EmP seasonal cycle, whereas evaporation is of secondary importance (not shown).

In general, the EmP annual cycle agrees well among four different data sets of 20CRv2, NCEP, ERA40, and OAFlux-GPCP. However, some discrepancies still exist. Net freshwater flux calculated from the OAFlux-GPCP precipitation displays an EmP ridge in July, which in turn leads to a weak semi-annual feature of EmP. 20CRv2 is a reanalysis data set which can best reproduce this phenomenon. The EmP ridge in July is predominated by the precipitation (not shown), which is closely related to the well-known phenomenon of the mid-summer drought that is more obvious in the regions of Central America and South Mexico (e.g. Magana et al. 1999; Mapes et al. 2005).

b. Processes controlling EmP seasonal cycle

Next we address how the EmP seasonal cycle is formed or what physical processes controlling the EmP seasonal cycle are. The left panels of Fig. 2 show EmP, the moisture tendency ($\partial \overline{W} / \partial t$), and the moisture flux divergence contributed from the monthly mean ($DivQ_M$) and from the transient eddies ($DivQ_E$). It is seen that the EmP seasonal cycle in the AWP region can be largely accounted for by $DivQ_M$, including moistening in the summer and fall and drying in the winter and spring, while the contribution from moisture tendency is negligible. Given the smallness of moisture tendency, this term is ignored in later discussions. In addition, we find that $DivQ_E$ also presents an annual cycle, which is almost in phase with EmP. The contribution from the transient eddies is significant in the summer (JJA), but with a smaller magnitude than the mean term of $DivQ_M$ in all other seasons. This is not surprising since the AWP resides over the tropics where atmospheric response to the ocean is primarily linear and baroclinic and the transient eddy is not very active.

As derived in Section 2, the change of $DivQ_M$ can be further separated into the thermodynamics contribution (δTH) and the contribution from the mean circulation dynamics (δMCD). The right panels of Fig. 2 show that a large portion of the EmP change can be explained by the mean circulation dynamics of δMCD , whereas the thermodynamics contribution of δTH is much smaller. δTH can be further decomposed into the effect of the change in humidity gradient when the advective wind is fixed at the climatological mean (δTH_A) and the effect of the change in humidity with a fixed climatological divergent wind (δTH_D) [see Eqs. (8) and (9)]. It can be found that δTH is primarily determined by δTH_A, while the contribution from δTH_D is negligible. Figure 2 shows that δTH_A is characterized by a net freshwater loss from the ocean in January-July and vice versa in August-December.

The mean circulation dynamics of δMCD is dominated by δMCD_D which represents the effect of change in the wind divergence with a fixed humidity as can be seen in Eq. (10). Clearly, the positive value of EmP in the winter and early spring (when the AWP disappears) is balanced by an increase in low-level wind divergence which disfavors precipitation and corresponds to a weakening of the ascent over the AWP region. The opposite is true during the summer and fall when the AWP appears. These results are consistent with previous modeling studies (e.g., Wang et al. 2008b) in which atmospheric response to a large (small) AWP is featured by an anomalous convergence (divergence) in the low level and an upward (a downward) vertical velocity – a classic Gill's pattern response to the tropical heating (Gill 1980).

The other component of δMCD_A is of secondary importance to the EmP change. Differing from other terms, δMCD_A shows a semi-annual feature, with a drying effect during the winter and summer and a moistening effect during the other seasons. This is also the determining factor to cause a weak semi-annual variability of EmP in 20CRv2 data set shown in Fig. 2a. In NCEP and ERA40, the contribution from δMCD_D is too strong to recognize the role of δMCD_A, so that a semi-annual variability of EmP does not seem to clearly show. It is expected that δMCD_A is largely associated with the wind change since the humidity gradient is fixed as shown in Eq. (11). Over the AWP region, the maximum of easterly zonal wind at 925 hPa occurs in the Caribbean region, which is called the Caribbean Low-Level Jet (CLLJ). As shown by Wang (2007), the CLLJ varies semi-annually, with two maxima in the summer and winter and two minima in the fall and spring. It is interesting to find that the semi-annual feature in δMCD_A is consistent with the variation of the CLLJ. This suggests that the CLLJ and the associated moisture transport may be closely related to the EmP variation, which will be examined in the following section. Wang (2007) further pointed out that the strength of the CLLJ is closely linked with the meridional SST gradient which is largely fluctuated with the AWP. Therefore, from the dynamical point of view, the AWP can not only induce an anomalous wind divergence to modulate EmP, but also modulate EmP by changing SST gradient to induce moisture advection by anomalous wind. Additionally, from the thermodynamical point of view, the AWP can modulate local EmP by changing humidity advection by the anomalous humidity gradient and by changing the water vapor content to affect the moisture divergence.

In summary, the EmP seasonal cycle associated with the AWP is dominated by the AWP-modulated mean circulation dynamics (δMCD), whereas the thermodynamics contribution (δTH) plays a much smaller role. Furthermore, the large contribution of the mean circulation dynamics is primarily due to the wind divergence change (δMCD_D).

c. Moisture transport across Central America

Our analysis in the previous section has suggested the potential importance of moisture advection by the CLLJ in the seasonal variation of the EmP over the AWP. In this sub-section, we address the CLLJ and its relationship with the moisture transport across Central America. Following previous studies (e.g., Wang 2007), we use the 925-hPa zonal wind in the region of 12.5°N-17.5°N, 80°W-70°W to measure the CLLJ. Figure 3 shows the seasonal variation of the CLLJ and the moisture transport from the Atlantic to the Pacific. All of the reanalysis data sets show a positive correlation between the CLLJ and the moisture transport contributed by the monthly mean part of MT_M. The linear correlation coefficient is 0.63, 0.60 and 0.62 for the 20CRv2, NCEP, and ERA40 reanalysis products, respectively. A strong (weak) CLLJ is associated with more (less) moisture export from the Atlantic to the Pacific. As expected, both the CLLJ and MT_M show a semi-annual feature, with two maxima in the winter and summer and two minima in the fall and spring. However, it can also be seen from Fig. 3 that the agreement between the two quantities in three reanalysis products is not perfect. The moisture transport contributed by the transient eddies is much smaller, which accounts for the total moisture transport by 6%, 4% and 2% in 20CRv2, NCEP and ERA40, respectively.

Eq. (12) shows that MT_M is dependent on the variation of $\overline{uq}$. Here we further decompose the $\overline{uq}$ change, $(\overline{uq})'$, into the following components (overbar is omitted):

$$(uq)' = u'q_M + u_M q' + u'q', \qquad (13)$$

where M denotes annual mean and the prime denotes the variation from the annual mean, i.e., $q' = q - q_M$. This decomposition allows us to separate the effects of humidity and wind changes (Fig. 4). All of three reanalysis products show that the moisture transport from the Atlantic to the Pacific is primarily determined by the wind change, whereas the contribution by the humidity change is small. The nonlinear term of $u'q'$ is very small and can be ignored. A comparison of Figs. 3 and 4 shows that the CLLJ and $u'q_M$ are in phase, again suggesting that the CLLJ is important for the moisture transport across Central America. In spite of small amplitude, the humidity change can still make contribution to the moisture transport. The contribution by the humidity change ($u_M q'$) is an increase (decrease) of moisture transport during the summer and fall (winter and spring) as a result of the appearance (disappearance) of the AWP.

We have shown a link among the AWP, EmP in the AWP region and the moisture transport across Central America. In association with the appearance (disappearance) of the AWP, less (more) moisture is exported from the Atlantic to the Pacific and more (less) precipitation occurs in the AWP region. This is because a large (small) AWP induces a low-level wind convergence (divergence) which favors (disfavors) local precipitation on one hand and also increases (decreases) the low-level westerly anomaly that decreases (increases) the moisture transport from the Atlantic to the Pacific on the other hand. However, there is an exception in July in which precipitation is less (Fig. 2) and more moisture is transported across Central America (Figs. 3-4) when the AWP is developed. This exception may result from the mid-summer drought, the CLLJ variation and the intrusion of the North Atlantic subtropical high. Finally, we would like to note that the magnitudes of the moisture transport across Central America and EmP over the AWP are comparable on seasonal timescale, implying that both of them can have a potential to affect ocean salinity (see next sub-section) and then the AMOC.

d. Seasonal cycle of sea surface salinity

The AWP-modulated EmP and moisture transport across Central America can ultimately affect ocean salinity, especially sea surface salinity (SSS). Figure 5 shows the seasonal SSS cycle averaged over the AWP region. As expected, SSS is small (large) during the summer and fall (winter and spring) when the AWP appears (disappears) and the EmP and moisture transport across Central America are small (large). However, we have to keep in mind that the seasonal cycle of mixed layer salinity also depends on salinity advection, especially in the eastern part of the AWP where horizontal salinity advection is very important (Foltz and McPhaden 2008). All the data sets of the direct observations and reanalysis products capture the seasonality of SSS in the AWP region although the detail is different. The SODA reanalysis product shares great similarity with the Argo observation, albeit with a smoother curve due to the relatively coarse resolution. This provides us a confidence to use SODA for analyzing the long-term variability of SSS in the following sections. SSS seasonality in GECCO and Ishii seems to be overestimated, while GFDL reanalysis tends to underestimate the SSS seasonal cycle over the AWP region.

4. Interannual variability

The freshwater flux in the AWP region also has significant interannual fluctuations. In this section, we examine and show the freshwater variability associated with the AWP, its associated mechanisms, moisture transport across Central America and SSS on interannual timescales.

a. EmP variability

We first compute the AWP index as the anomalies of the area of SST warmer than 28.5°C divided by the climatological AWP area (Wang et al. 2006, 2008a), as shown in Fig. 6a. The interannual AWP variability (Fig. 6b) is obtained by performing an 8-year high frequency filter to the detrended AWP index. We identify a warm pool 25% larger (smaller) than the climatological area as a large (small) warm pool; otherwise, warm pool is classified as normal or neutral. Given that the AWP almost does not exist during the winter and spring based on the definition of SST warmer than 28.5°C, we attempt to highlight the EmP anomalies associated with the AWP in the summer (JJA) and fall (SON). The composites of the EmP anomalies for the large and small AWP (LAWP and SAWP) are shown in Fig. 7. All of the data sets show a similar pattern during JJA. The entire TNA experiences a reduced EmP when the AWP is large, with maximum values located in the AWP and the eastern ITCZ region, whereas there is an increased EmP in the west of subtropical North Atlantic and the tropical South Atlantic (the left panels of Fig. 7). The opposite is true for SAWP (the right panels of Fig. 7). The largest EmP anomalies in the AWP region can attain 0.8 mm/day. This indicates that the tropical North Atlantic Ocean is occupied by freshwater excess (deficit) when the AWP is large (small). During the fall, the EmP anomalies show similar response to that during the summer (not shown). Therefore, we only show and discuss plots during the summer in the following sections.

We also compute the time series of the EmP anomalies in the region of 5°-30°N from the American coast to 40°W and then compare it with the AWP index (Fig. 6). The first impression from Fig. 6 is that different data sets show different variations of the EmP anomalies. However, on interannual timescales all time series of the EmP anomalies show an out-of-phase relationship with the AWP index (Fig. 6b), with a large (small) AWP coinciding with a gain (loss) of freshwater to the ocean. This is consistent with the composite analysis in Fig. 7. The correlation coefficients are -0.40, -0.57, -0.36, and -0.50 in 20CRv2, NCEP, ERA40 and OAFlux-GPCP, respectively, all of which are significant at the 95% confidence level.

b. Processes controlling the EmP anomalies

As shown in Eqs. (2) and (5), the EmP anomalies are mainly determined by the changes contributed by the moisture divergence from the monthly mean [$\delta(DivQ_M)$] and the transient eddies [$\delta(DivQ_E)$]. $\delta(DivQ_M)$ can be further decomposed into the thermodynamics contribution (δTH) and the mean circulation dynamics contribution (δMCD). The composites of these terms for the large and small AWPs during JJA are shown in Fig. 8 based on the 20CRv2 data set. Note that the ERA40 and NCEP data sets are also analyzed, showing similar patterns to the 20CRv2 data set. Since the 20CRv2 has much longer period than the ERA40 and NCEP, we only present the results from the 20CRv2. A large portion of the EmP anomalies in the tropical Atlantic (Figs. 7a, b) can be accounted for by the moisture flux divergence variation of $DivQ_M$ (Figs. 8a, b). The transient eddies of $DivQ_E$ play a much smaller role than $DivQ_M$ in the AWP region (Figs. 8c, d). However, the transient eddies do contribute to the EmP variability in the middle and high latitudes. This is an expected result since eddy is more active in high latitudes than low latitudes. A further calculation shows that the mean circulation dynamics contribution of δMCD is a major contributor to the variation of $DivQ_M$ (Figs. 8e, f), while the role of δTH is very small (Figs. 8g, h).

δMCD is contributed by the terms due to the wind divergence change (δMCD_D) and the wind advection of humidity (δMCD_A). Figures 9a-d show that δMCD_D is a dominant term, whereas δMCD_A is secondary. Given the dramatic decrease in specific humidity with height, the δMCD_D anomalies may come mainly from the low troposphere. In fact, the composites of the 925-hPa wind divergence anomalies for the large and small AWPs do confirm the result (Figs. 9e, f). During the large (small) AWPs, the low-level anomalous convergence (divergence) is associated with anomalous ascent (descent) in the middle troposphere (not shown) which decreases (increases) the EmP anomalies. The change of δMCD_A reflects primarily the change in low-level winds (Figs. 9g, h). Due to the small climatological humidity gradient in the AWP region, the wind changes do not induce a large contribution to the EmP anomalies. Figures 9g and h show that in association with the large (small) AWPs, the CLLJ is significantly weakened (strengthened), implying that less (more) moisture is transported from the tropical Atlantic to the Pacific (which will be discussed and shown next).

d. Moisture transport anomalies across Central America

The composite analyses of the moisture transport anomalies across Central America for the large and small AWPs based on different data sets are shown in Fig. 10. All of the three reanalysis products show a consistent result, albeit with the difference in the transport magnitude. A large (small) AWP is associated with the negative (positive) moisture transport anomalies or less (more) moisture transport from the Atlantic to the Pacific. Like the seasonal cycle, this moisture transport response is dominated by the wind change associated with the CLLJ variation (Fig. 9), whereas the specific humidity plays a minor and opposite contribution. This is easily understood. Due to the nonlinearity of the Clausius-Clapeyron equation, the specific humidity increases more over warm water than over cool water in the absence of any sizable change in relative humidity. Hence, moisture becomes increased (decreased) in response to a large (small) AWP, which in turn favors more (less) moisture transported to the Pacific. However, the specific humidity response cannot be overwhelmed by the role of wind change which tends to reduce (increase) the easterly wind and thus generate a weakened (strengthened) moisture transport across Central America during a large (small) AWP. Note that the magnitude (peak-to-peak variation) of interannual moisture transport anomalies associated with the AWP is about 0.06 Sv which is much smaller than the long-term mean (0.26 Sv averaged in the three reanalysis products) and the seasonal cycle (0.4 Sv).

d. SSS anomalies

As expected, SSS is characterized by the negative (positive) anomalies over the AWP region for a large (small) AWP in both the SODA reanalysis and Ishii salinity data (Fig. 11). The SSS anomalies are consistent with the EmP response and moisture transport change across Central America (Fig. 7). This indicates that, to the first order, SSS variability over the AWP region associated with the AWP on the interannual timescales is balanced by the local freshwater flux. When the AWP is large (small), there is an anomalous low-level convergence (divergence) over the AWP region on one hand and a weakened (strengthened) trade wind across Central America on the other hand. The former tends to increase (decrease) precipitation and the latter tends to decrease (increase) the moisture transport across Central America leading more (less) water vapor resided in the AWP region. Both of these two effects are in favor of generating the negative (positive) SSS anomalies in the AWP region when the AWP is large (small).

5. Multidecadal variability

As shown in Fig. 6c, the EmP anomalies in the AWP region also vary on multidecadal timescales, with the positive (negative) EmP anomalies coinciding with the small (large) AWP. Using the multidecadal AWP index, we identify the positive (negative) phase of the AWP as AWP^+ (AWP^-) by a warm pool 10% larger (smaller) than the climatological mean. We then investigate the relationship of the EmP anomalies with the AWP on multidecadal timescales by making composites. As shown in Fig. 12, there is a net freshwater gain over the TNA during the warm phase of the AWP, particularly in the AWP and tropical eastern North Atlantic regions, and the opposite occurs during the cold phase of the AWP. Compared to the EmP variation on interannual timescales, the multidecadal variability of EmP exhibits a relatively smaller magnitude (Fig. 7 vs Fig. 12), which is also revealed in the time series (Figs. 6b, c) (but the multidecadal variability may be very important since it persists on a longer timescale). Similar to the interannual variability, the multidecadal change of EmP in the tropical Atlantic is balanced mainly by the moisture flux divergence of $DivQ_M$ (Figs. 13a, b), whereas the contribution from the transient eddies of $DivQ_E$ is very small (Figs. 13c, d). Again, the mean circulation dynamics of δMCD is a major contributor to $DivQ_M$, whereas the thermodynamics contribution of δTH is very small (Figs. 13e-h). The contribution to the mean circulation dynamics primarily arises from δMCD_D (Figs. 14a, b) and δMCD_A is small and even opposite (Figs. 14c, d).

The effect of δMCD_D is also seen from the low-level anomalous wind divergence field (Figs. 14e, f). The tropical Atlantic is characterized by a dipole divergence field anomaly, with an anomalous convergence in the north and an anomalous divergence in the south during the warm phase of the AWP, and vice versa during the cold phase of the AWP. This implies that the ITCZ has shifted toward north (south) during the warm (cold) phase of the AWP. In association with the ITCZ shift, the Hadley circulation cell also shows a change. Figure 15 shows the climatological Hadley cell together with the change from the cold to warm phases to the AWP. It is clearly seen that the climatological Hadley cell ascends to the upper level around 10°N, diverges to the north and south when it reaches to the upper layer, and ultimately descends to the lower level at about 30°N. The difference between the AWP warm and cold phases shows the negative streamfunction anomalies over the climatological ascent region, indicating a northward (southward) shift of the Hadley cell.

Similar to the interannual variability, δMCD_A mainly reflects the changes in the low-level wind. As exhibited in Figs. 14g, h, the poleward flow corresponds to the negative EmP anomalies and the equatorward flow is associated with the positive EmP anomalies. A large (small) AWP on multidecadal timescales also coincides with a weakened (strengthened) CLLJ.

As expected, both the moisture transport and SSS on multidecadal timescales show a similar response to the interannual variation (Figs. 16 and 17). The moisture transport from the tropical Atlantic to the Pacific is also characterized by a reduced (an increased) transport across Central America during the warm (cold) phase of the AWP (Fig. 16). However, the amplitude of the multidecadal moisture transport is smaller than the interannual variation because of a small response of the CLLJ. Consistent with the distribution of the EmP anomalies and the moisture transport across Central America, the multidecadal SSS variability shows the negative (positive) anomalies in the AWP region.

6. Summary and discussion

The paper uses various reanalysis products and observations to examine the response of freshwater flux and SSS to the AWP variability. All of the data sets show consistent and similar results for the variations of seasonal, interannual and multidecadal timescales. A large (small) AWP is associated with an increased (decreased) freshwater gain (loss) to the ocean, which is primarily due to the negative (positive) EmP anomalies and the decreased (increased) moisture transport from the Atlantic to Pacific basins across Central America. The moisture budget analyses show that the EmP anomalies are mainly balanced by the moisture flux divergence change primarily from the monthly to longer timescales, whereas the contribution from the transient eddies is much smaller. The moisture flux divergence change arises mainly from the change of the mean circulation dynamics (change in wind but no change in humidity), while the thermodynamics contribution (change in humidity but no change in wind) is of secondary importance. A further decomposition of the mean circulation dynamics demonstrates that the wind divergent change plays a dominant role and the advection of moisture by the wind change is small. Consistent with previous modeling study (Wang et al. 2008b), the wind divergent change results from the warm SST anomalies in the AWP region. When the AWP is large (small), warm (cold) SST over the AWP region induces an anomalous convergence (divergence) in the low level according to Gill's (1980) theory, which induces an anomalous ascent (descent) motion and thus generates an increased (decreased) precipitation. Meanwhile, the divergent circulation change is associated with the north-south shift of the ITCZ, leading to an anomalous precipitation band over the tropical Atlantic.

On the other hand, a large (small) AWP is also associated with a weakening (strengthening) of the CLLJ and the westerly (easterly) anomalies across Central America. The wind change reduces (enhances) the moisture transport from the Atlantic to the Pacific, which in turn leads to more (less) moisture resided in the AWP region and thus generates more (less) local precipitation. Both the local EmP and moisture transport changes can affect the ocean salinity ultimately. As expected, SSS variability associated with the AWP is characterized by the negative (positive) SSS anomaly response to a large (small) AWP.

Although the features and processes of the freshwater variations in the AWP are similar on seasonal, interannual and multidecadal timescales, their magnitudes are quite different. The range or amplitude (peak-to-peak variation) of the AWP-modulated seasonality of the EmP anomalies has the largest value, reaching to 0.6 Sv. The magnitude of interannual variability of EmP associated with the AWP in the summer is about 0.2 Sv, while the multidecadal variability has a smaller amplitude which can reach to 0.15 Sv. Similarly, the moisture transport across Central America associated with the AWP has the largest magnitude in the seasonal cycle which can reach to 0.4 Sv. However, the cross-Central American moisture transport exhibits a smaller amplitude change in the summer on the interannual and multidecadal timescales, with amplitude about 0.06 Sv and 0.02 Sv, respectively. As a result, SSS has the largest amplitude in the seasonal cycle (0.6 psu), however, it only has 0.4 psu and 0.2 psu fluctuations on interannual and multidecadal timescales, respectively.

The results suggest a potential interaction between the AWP and the Atlantic meridional overturning circulation (AMOC) through the freshwater and salinity response. On one hand, as the AMOC weakens, its northward heat transport reduces and thus the North Atlantic cools and the AWP becomes small. On the other hand, a small AWP decreases rainfall in the TNA and increases the cross-Central American moisture export to the eastern North Pacific. Both of these factors tend to increase salinity in the tropical North Atlantic Ocean. Advected northward by the wind-driven ocean circulation (Thorpe et al. 2001; Vellinga and Wu 2004; Yin et al. 2006; Krebs and Timmermann 2007), the positive salinity anomalies may increase the upper-ocean density in the deep-water formation regions and thus strengthens the AMOC. Therefore, the AWP seems to play a negative feedback role that acts to restore the AMOC after it is weakened or shut down. This hypothesis needs to be tested and confirmed by using numerical model experiments. In particular, model experiments should address whether the AWP-related freshwater flux and the moisture export across Central America to the eastern Pacific are of significance for the strength of the AMOC, if the persistence of the anomaly is on a longer timescale (say, on the order of decades).

Acknowledgments. We thank Greg Foltz for serving as AOML's internal reviewer and two anonymous reviewers for their comments and suggestions. This work was supported by grants from National Oceanic and Atmospheric Administration (NOAA) Climate Program Office, the base funding of NOAA Atlantic Oceanographic and Meteorological Laboratory (AOML). The findings and conclusions in this report are those of the author(s) and do not necessarily represent the views of the funding agency.

References

Adler, R. F., and Coauthors, 2003: The Version-2 Global Precipitation Climatology Project (GPCP) monthly precipitation analysis (1979–present). *J. Hydrometeor.,* **4**, 1147–1167.

Broecker, W. S., 1997: Thermohaline circulation, the Achilles heel of our climate system: will man-made CO2 upset the current balance? *Science*, **278**, 1582–1588.

Carton, J. A., and B. S. Giese, 2008: A reanalysis of ocean climate using Simple Ocean Data Assimilation (SODA). *Mon. Weather Rev*., **136**, 2999–3017.

Compo, G. P. and Coauthors, 2011: The Twentieth Century Reanalysis Project. *Quart. J. Roy. Meteor. Soc.*, **137**, 1–28.

Foltz, G. R., and M. J. McPhaden, 2008: Seasonal mixed layer salinity balance of the tropical North Atlantic Ocean. *J. Geophys. Res*., **113**, C02013, doi:10.1029/2007JC004178.

Gibson, J. K., P. Kållberg, S. Uppala, A. Nomura, A. Hernandez, and E. Serrano, 1997: ERA description. ECMWF Re-Analysis Project Report Series, No. 1, ECMWF, Reading, United Kingdom, 71 pp.

Gill, A. E., 1980: Some simple solutions for heat-induced tropical circulation. *Quart. J. Roy. Meteor. Soc*., **106**, 447-462.

Ishii, M., M. Kimoto, K. Sakamoto, and S. I. Iwasaki, 2006: Steric sea level changes estimated from historical ocean subsurface temperature and salinity analyses. *J. Oceanography*., **62** (2), 155-170.

Katsumata, K., and H. Yoshinari, 2010: Uncertainties in global mapping of Argo drift data at the parking level. *Journal of Oceanography.,* **66**, 553-569.

Kalnay, E., and Coauthors, 1996: The NCEP/NCAR 40-Year Reanalysis Project. *Bull. Amer.*

Meteor. Soc., **77**, 437–471.

Kõhl, A., D. Dommenget, K. Ueyoshi, and D. Stammer, 2006: The Global ECCO 1952 to 2001 Ocean Synthesis. Tech. Rep. 40, 43 pp. [Available online at http://www.ecco-group.org/ecco1/report/report_40.pdf.]

Krebs, U., and A. Timmermann, 2007: Tropical air-sea interactions accelerate the recovery of the Atlantic Meridional Overturning Circulation after a major shutdown. *J. Climate*, **20**, 4940–4956.

Magana V., J. A. Amador, and S. Medina, 1999: The midsummer drought over Mexico and Central America. *J. Climate*, **12**, 1577–1588.

Mapes, B. E., P. Liu, and N. Buenning, 2005: Indian monsoon onset and the Americas midsummer drought: out-of-equilibrium response to smooth seasonal forcing. *J Climate*, **18**, 1109–1115.

Peixoto, J. P., and A. H. Oort, 1992: *Physics of Climate*. *American Institute of Physics.,* 520 pp.

Romanova, V., M. Prange, and G. Lohmann, 2004: Stability of the glacial thermohaline circulation and its dependence on the background hydrological cycle. *Clim. Dyn.,* **22**, 527–538.

Rosati, A., M. Harrison, A. Wittenberg, and S. Zhang, 2004: NOAA/GFDL ocean data assimilation activities. CLIVAR Workshop on Ocean Reanalysis, 9 November 2004. NCAR, Boulder.

Richter, I., and S.-P. Xie, 2010: Moisture transport from the Atlantic to the Pacific basin and its response to North Atlantic cooling and global warming. *Clim. Dyn.*, **35** (2), 551–566.

Seager, R., N. Naik, and G. A. Vecchi, 2010: Thermodynamic and dynamic mechanisms for large-scale changes in the hydrological cycle in response to global warming. *J Climate*, **23**, 4651–4668.

Thorpe, R. B., and Coauthors, 2001: Mechanisms determining the Atlantic thermohaline circulation response to greenhouse gas forcing in a non-flux-adjusted coupled climate model. *J. Climate*, **14**, 3102-3116.

Trenberth, K. E., and C. J. Guillemot, 1995: Evaluation of the global atmospheric moisture budget as seen from analyses. *J Climate*, **8**, 2255-2272.

Vellinga, M., and P. Wu, 2004: Low-latitude freshwater influences on centennial variability of the Atlantic thermohaline circulation. *J. Climate*, **17**, 4498–4511.

Wang, C., and D. B. Enfield, 2001: The tropical Western Hemisphere warm pool. *Geophys. Res. Lett.*, **28**, 1635-1638.

Wang, C., and D. B. Enfield, 2003: A further study of the tropical Western Hemisphere warm pool. *J. Climate*, **16**, 1476-1493.

Wang, C., D. B. Enfield, S.-K. Lee, and C. W. Landsea, 2006: Influences of the Atlantic warm pool on Western Hemisphere summer rainfall and Atlantic hurricanes. *J. Climate*, **19**, 3011-3028.

Wang, C., 2007: Variability of the Caribbean low-level jet and its relations to climate. *Clim. Dyn.*, **29**, 411-422.

Wang, C., and S.-K. Lee, 2007: Atlantic warm pool, Caribbean low-level jet, and their potential impact on Atlantic hurricanes. *Geophys. Res. Lett.*, **34**, L02703, doi:10.1029/2006GL0028579.

Wang, C., S.-K. Lee, and D. B. Enfield, 2007: Impact of the Atlantic warm pool on the summer climate of the Western Hemisphere. *J. Climate*, **20**, 5021-5040.

Wang, C., S.-K. Lee, and D. B. Enfield, 2008a: Atlantic Warm Pool acting as a link between Atlantic Multidecadal Oscillation and Atlantic tropical cyclone activity. *Geochem. Geophys. Geosyst.*, **9**, Q05V03, doi:10.1029/2007GC001809.

Wang, C., S.-K. Lee, and D. B. Enfield, 2008b: Climate response to anomalously large and small Atlantic warm pools during the summer. *J. Climate*, **21**, 2437-2450.

Xie, P., and P. A. Arkin, 1997: Global precipitation: A 17-year monthly analysis based on gauge observations, satellite estimates, and numerical model outputs. *Bull. Amer. Meteor. Soc.*, **78**, 2539–2558.

Yin, J., M. E. Schlesinger, N. G. Andronova, S. Malyshev, and B. Li, 2006: Is a shutdown of the thermohaline circulation irreversible? *J. Geophys. Res*., **111**, D12104, doi:10.1029/2005JD006562.

Yu, L., and R. A. Weller, 2007: Objectively analyzed air-sea heat flux for the global ice-free oceans (1981-2005). *Bull. Amer. Meteor. Soc*., **88**, 527-539.

Zaucker, F., and W. S. Broecker, 1992: The influence of atmospheric moisture transport on the fresh water balance of the Atlantic drainage basin: general circulation model simulations and observations. *J. Geophys. Res*., **97**, 2765–2773.

Figure Captions

Figure 1. ETOP05 orography (m, shading) and the line segments across which moisture transport is calculated (black line). ETOPO5 was generated from a digital data base of land and sea-floor elevations on a 5-minute latitude/longitude grid (which can be downloaded from http://www.usgodae.org/pub/outgoing/static/ocn/bathy/).

Figure 2. EmP seasonal cycle (left panels) and associated moisture budget (right panels) using the (a, b) 20CRv2, (c, d) NCEP, (e, f) ERA40 and (g) OAFlux-GPCP data sets. *EmP*, W_t, $DivQ_M$ and $DivQ_E$ denote the EmP, moisture tendency, and moisture flux divergence contribution from monthly to longer timescales and moisture flux divergence contribution from the transient eddies (sub-monthly time scale), respectively. The AWP area (10^{12} m^2) of SST larger than 28.5°C is also shown in (g). The right panels represent the contributions from the mean circulation dynamics (δMCD) and thermodynamics (δTH) and their corresponding advective parts (δMCD_A, δTH_A) and convergent parts (δMCD_D, δTH_D). Unit is Sv (1 Sv=10^6 m^3/s=10^9 kg/s). The AWP region is in the region of 5°N-30°N from the America coast to 40°W.

Figure 3. Seasonal cycle of the moisture transport (*MT*) across Central America and the CLLJ in (a) 20CRv2, (b) NCEP and (c) ERA40. The moisture transport contributed by the monthly to longer timescales is denoted as mean (blue line) and by the transient eddies (sub-monthly timescales) is represented as eddy (green line). The positive value represents an easterly wind of the CLLJ and a moisture transport from the Atlantic to the Pacific basin.

Figure 4. Seasonal cycle of the moisture transport (monthly and longer timescale part) variations across Central America and the associated decomposed components in (a) 20CRv2, (b) NCEP and (c) ERA40.

Figure 5. Seasonal cycle of sea surface salinity (SSS) over the AWP region based on various data sets of SODA, GECCO, GFDL and Argo observations and WOA data developed by Ishii et al. (2006).

Figure 6. Time series of the AWP area index (100%) and the integrated EmP anomalies (Sv) over the AWP region during the summer (JJA). The AWP area index is calculated by the ERSST data, and the EmP anomalies are based on the data sets of 20CRv2, NCEP, ERA40, and OAFlux-GPCP. Shown are the (a) total, (b) interannual and (c) longer-term (decadal and multidecadal) variability. The interannual (longer-term) variability is obtained by performing an 8-year high (low) frequency filter to the detrended time series. In (c), the only 20CRv2 EmP time series is shown since other data sets are too short to examine longer-term variations.

Figure 7. Composites of the EmP anomalies (mm/day) on interannual timescales during the summer (JJA). Shown are for large AWP (left panels) and small AWP (right panels) from various data sets of (a, b) 20CRv2, (c, d) NCEP, (e, f) ERA40 and (g, h) OAFlux-GPCP.

Figure 8. Composites of the moisture flux divergence anomalies on interannual timescales for large AWP (left panels) and small AWP (right panels) during the summer (JJA). Shown are the moisture flux divergence from (a, b) monthly to longer timescales of $DivQ_M$ and from (c, d) the transient eddies of $DivQ_E$. $DivQ_M$ is further decomposed into (e, f) the mean circulation dynamics contribution of δMCD and (g, h) the thermodynamics contribution of δTH. Unit is mm/day. The composites are calculated based on 20CRv2.

Figure 9. Composites of the moisture change (mm/day) due to mean circulation dynamics on interannual timescales for large AWP (left panels) and small AWP (right panels) during the summer (JJA). Shown are the contribution by (a, b) the wind divergent change and (c, d) the advection of moisture by the wind change. Composites of the 925-hPa wind divergence and wind anomalies are shown in (e, f) and (g, h), respectively. The composites are calculated based on 20CRv2.

Figure 10. Composites of the cross-Central America moisture transport anomalies on interannual timescales for large AWP and small AWP during the summer (JJA) using the data sets of 20CRv2, NCEP and ERA40.

Figure 11. Composites of the sea surface salinity (SSS) anomalies (psu) on interannual timescales for large AWP and small AWP during the summer (JJA) based on the SODA and Ishii data.

Figure 12. Composites of the EmP anomalies (mm/day) on multidecadal timescales during the summer (JJA). Shown are for the positive phase of the AWP (left panels) and the negative phase of the AWP (right panels) from the data sets of (a, b) 20CRv2 and (c, d) NCEP.

Figure 13. Composites of the moisture flux divergence anomalies on multidecadal timescales during the summer (JJA) for the positive phase of the AWP (left panels) and the negative phase of the AWP (right panels). Shown are the moisture flux divergence from (a, b) monthly to longer timescales of $DivQ_M$ and from (c, d) the transient eddies of $DivQ_E$. $DivQ_M$ is further decomposed into (e, f) the mean circulation dynamics contribution of δMCD and (g, h) the thermodynamics contribution of δTH. Unit is mm/day. The composites are calculated based on 20CRv2.

Figure 14. Composites of the moisture change (mm/day) due to the mean circulation dynamics on multidecadal timescales during the summer (JJA) for the positive phase of the AWP (left panels) and the negative phase of the AWP (right panels). Shown are the contribution by (a, b) the wind divergent change and (c, d) the advection of moisture by the wind change. Composites of the 925-hPa wind divergence and wind anomalies are shown in (e, f) and (g, h), respectively. The composites are calculated based on 20CRv2.

Figure 15. The Hadley circulation during the summer (JJA) defined as the zonal mean

stream function in 20CRv2. The contour lines represent the climatological Hadley cell and the shading denotes the difference of the Hadley cell between the positive and negative phases of the AWP on multidecadal timescales. Contour interval is 20×10^9 kg s^{-1}.

Figure 16. Composites of the cross-Central America moisture transport anomalies (Sv) on multidecadal timescales during the summer (JJA) for the positive and negative phases of the AWP using the data sets of 20CRv2 and NCEP.

Figure 17. Composites of the sea surface salinity (SSS) anomalies (psu) on multidecadal timescales during the summer (JJA) for the positive phase of the AWP (left panels) and the negative phase of the AWP (right panels) based on the SODA and Ishii data.

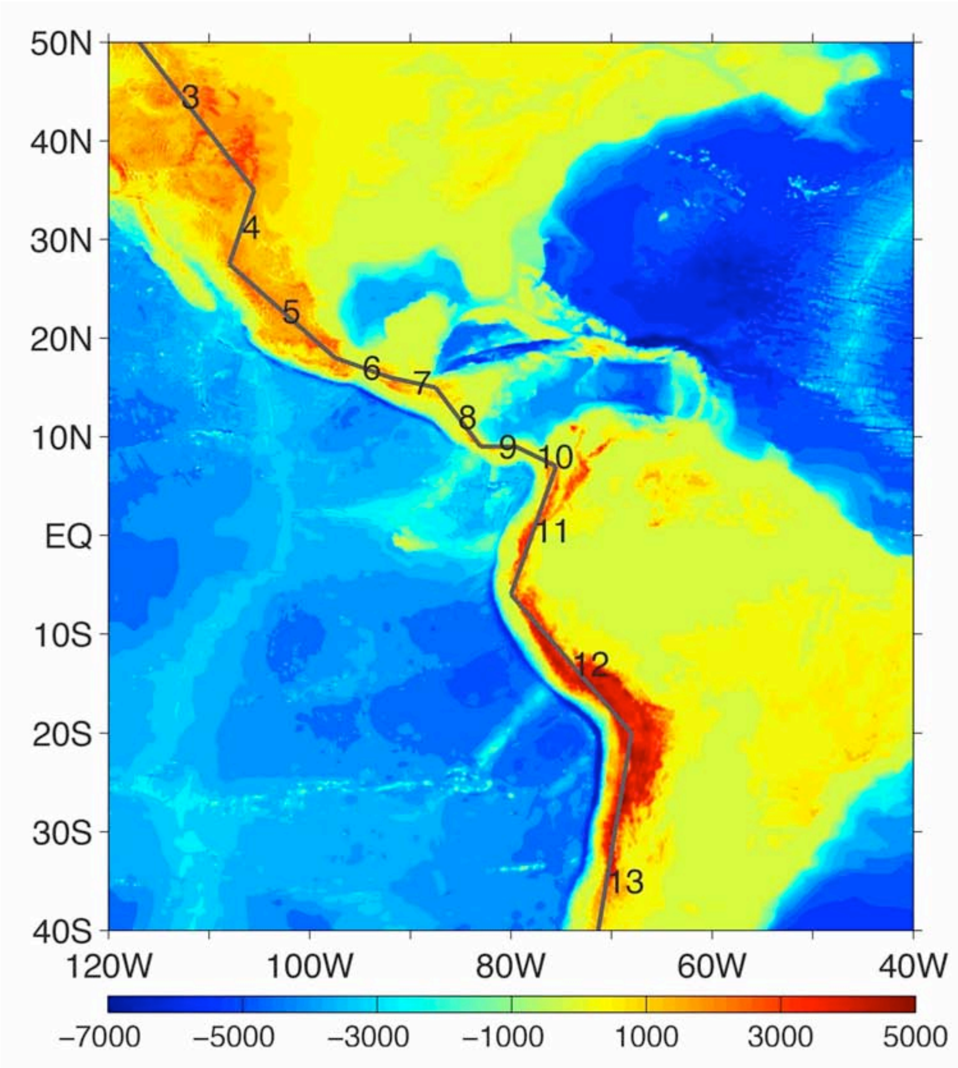

Figure 1. ETOP05 orography (m, shading) and the line segments across which moisture transport is calculated (black line). ETOPO5 was generated from a digital data base of land and sea-floor elevations on a 5-minute latitude/longitude grid (which can be downloaded from http://www.usgodae.org/pub/outgoing/static/ocn/bathy/).

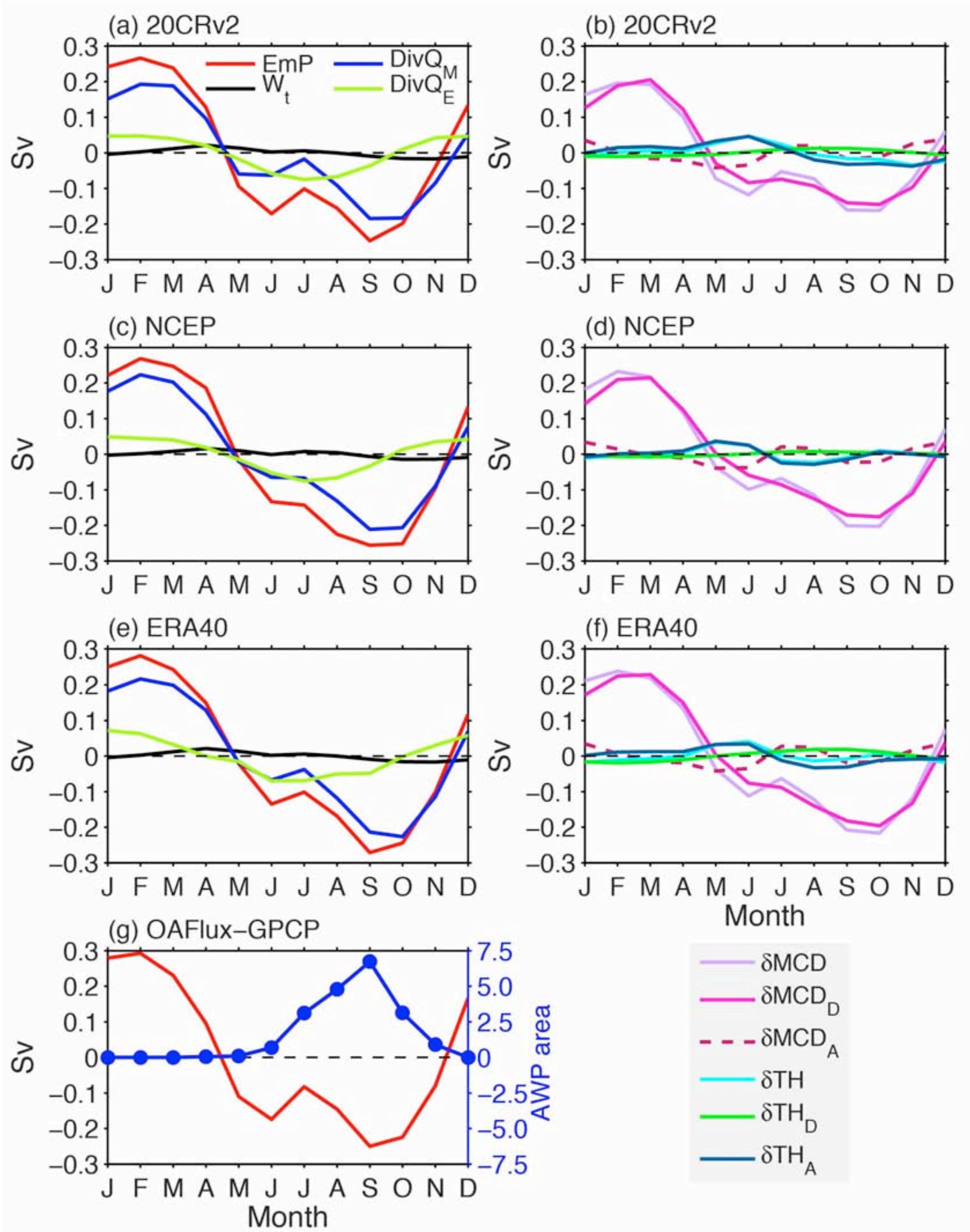

Figure 2. EmP seasonal cycle (left panels) and associated moisture budget (right panels) using the (a, b) 20CRv2, (c, d) NCEP, (e, f) ERA40 and (g) OAFlux-GPCP data sets. *EmP*, W_t, $DivQ_M$ and $DivQ_E$ denote the EmP, moisture tendency, and moisture flux divergence contribution from monthly to longer timescales and moisture flux divergence contribution from the transient eddies (sub-monthly time scale), respectively. The AWP area (10^{12} m^2) of SST larger than 28.5°C is also shown in (g). The right panels represent the contributions from the mean circulation dynamics (δMCD) and thermodynamics (δTH) and their corresponding advective parts (δMCD_A, δTH_A) and convergent parts (δMCD_D, δTH_D). Unit is Sv (1 Sv=10^6 m^3/s=10^9 kg/s). The AWP region is in the region of 5°N-30°N from the America coast to 40°W.

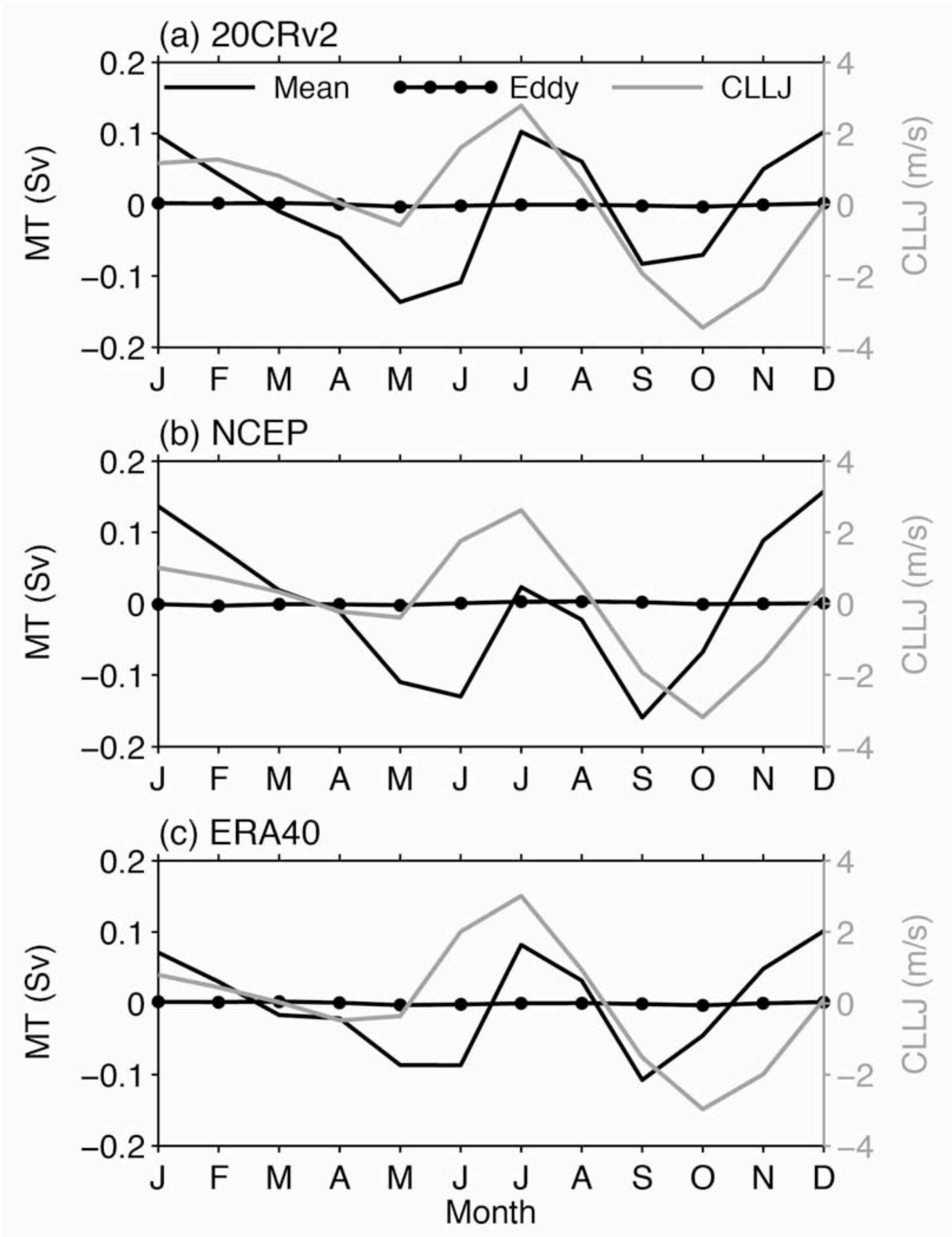

Figure 3. Seasonal cycle of the moisture transport (*MT*) across Central America and the CLLJ in (a) 20CRv2, (b) NCEP and (c) ERA40. The moisture transport contributed by the monthly to longer timescales is denoted as mean (blue line) and by the transient eddies (sub-monthly timescales) is represented as eddy (green line). The positive value represents an easterly wind of the CLLJ and a moisture transport from the Atlantic to the Pacific basin.

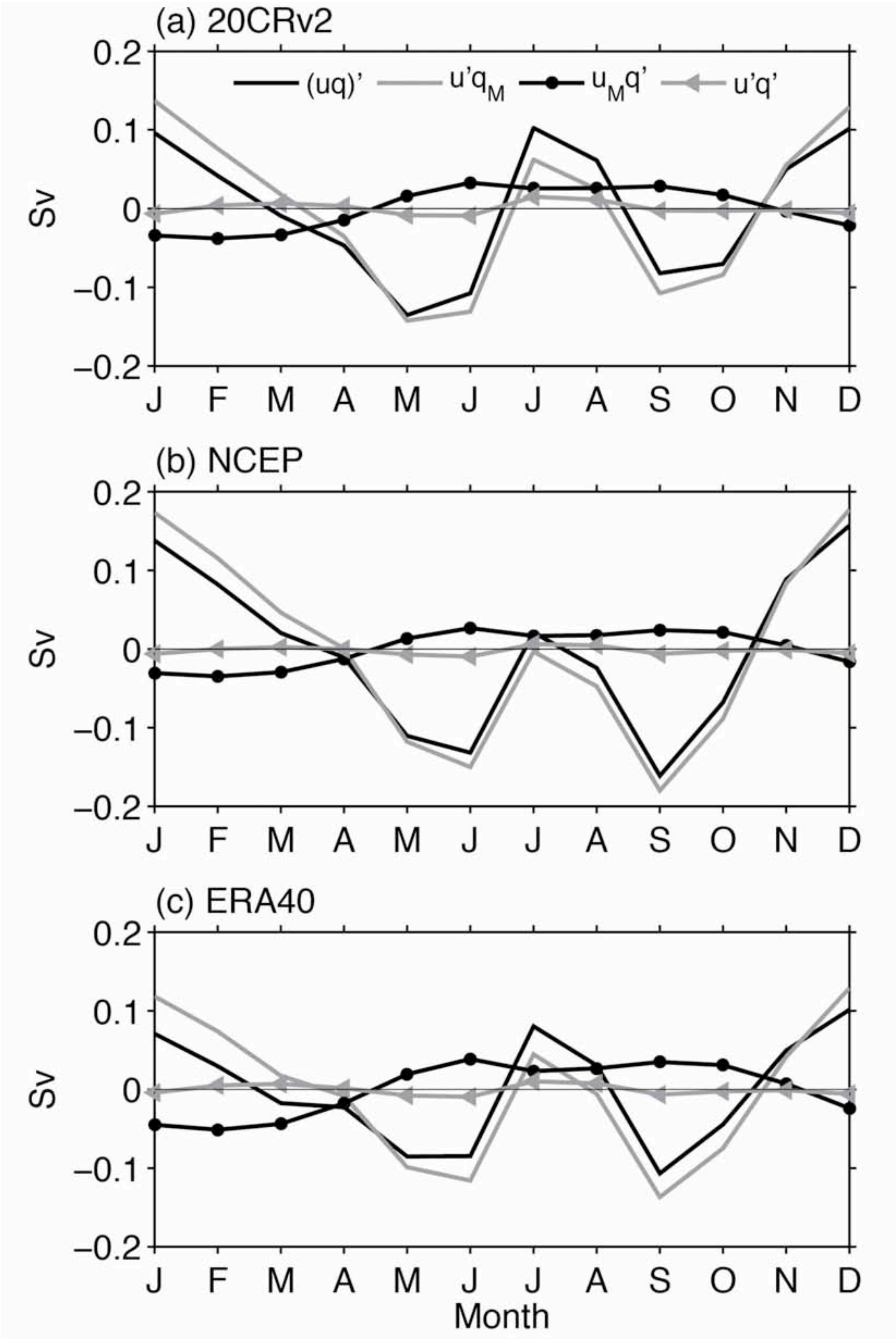

Figure 4. Seasonal cycle of the moisture transport (monthly and longer timescale part) variations across Central America and the associated decomposed components in (a) 20CRv2, (b) NCEP and (c) ERA40.

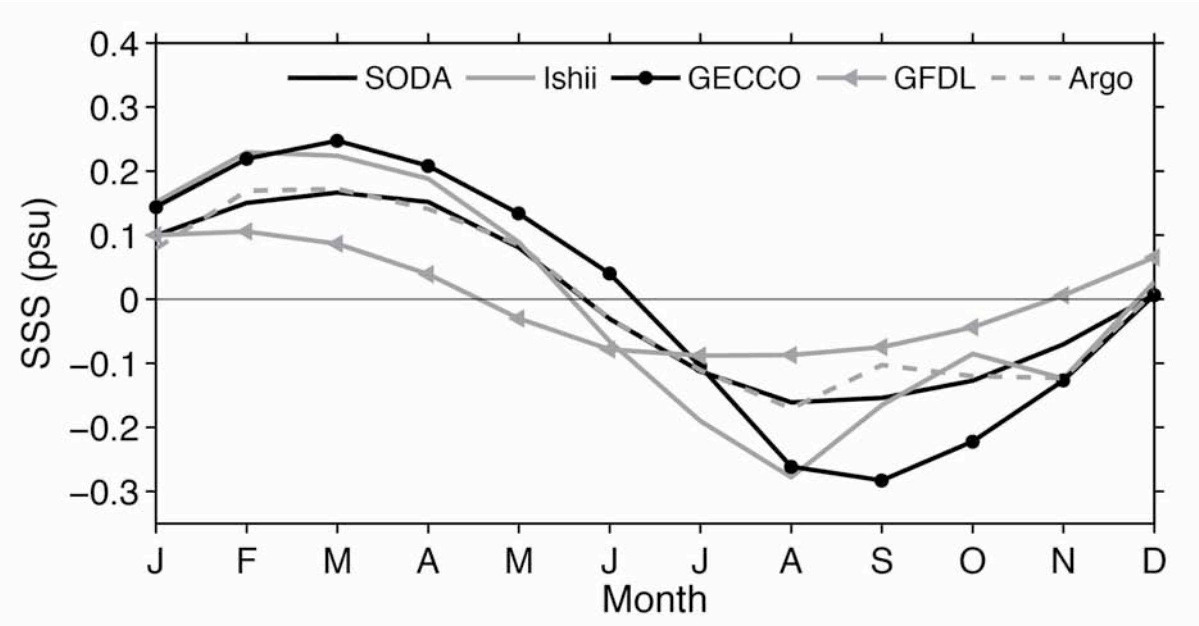

Figure 5. Seasonal cycle of sea surface salinity (SSS) over the AWP region based on various data sets of SODA, GECCO, GFDL and Argo observations and WOA data developed by Ishii et al. (2006).

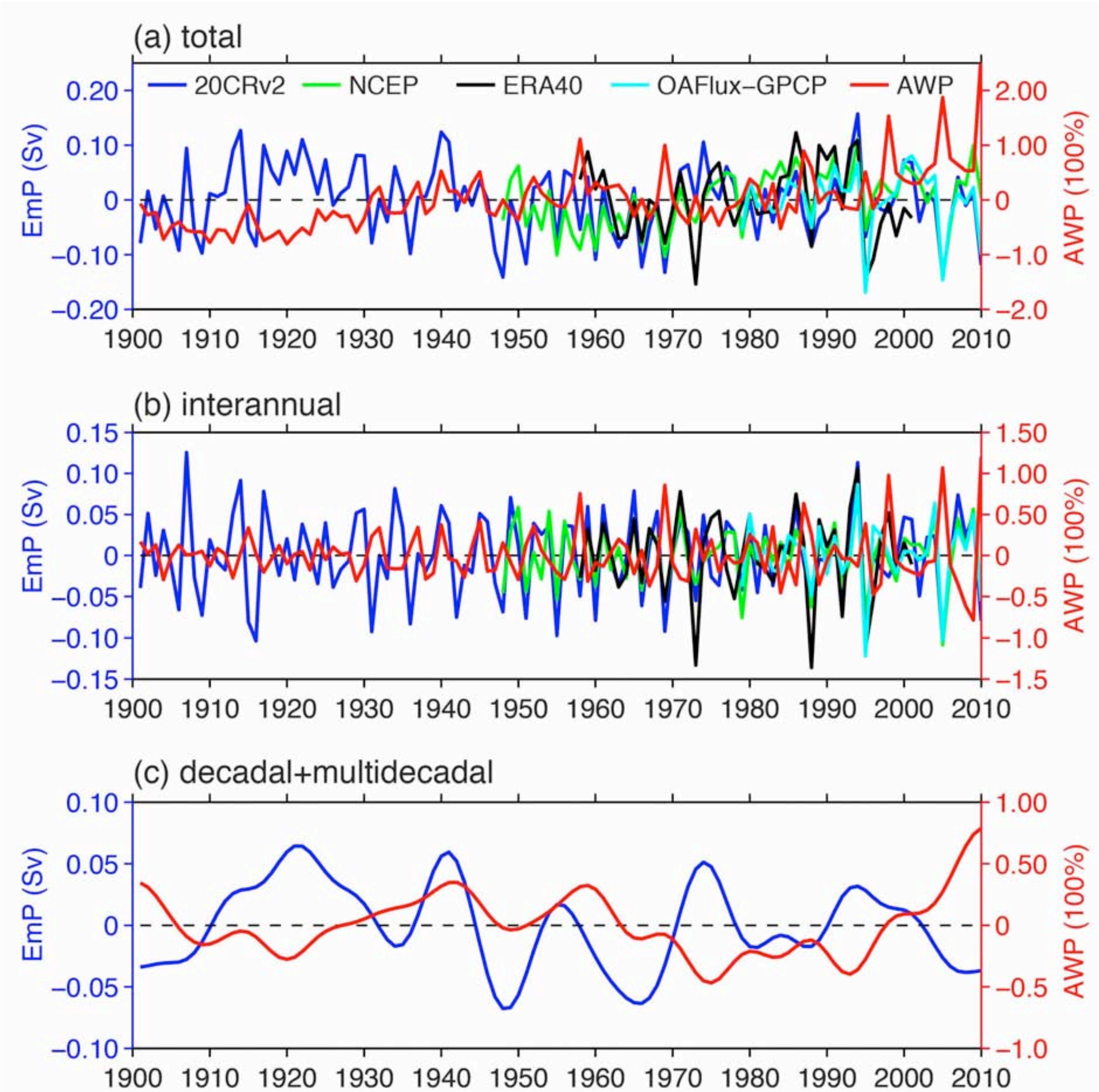

Figure 6. Time series of the AWP area index (100%) and the integrated EmP anomalies (Sv) over the AWP region during the summer (JJA). The AWP area index is calculated by the ERSST data, and the EmP anomalies are based on the data sets of 20CRv2, NCEP, ERA40, and OAFlux-GPCP. Shown are the (a) total, (b) interannual and (c) longer-term (decadal and multidecadal) variability. The interannual (longer-term) variability is obtained by performing an 8-year high (low) frequency filter to the detrended time series. In (c), the only 20CRv2 EmP time series is shown since other data sets are too short to examine longer-term variations.

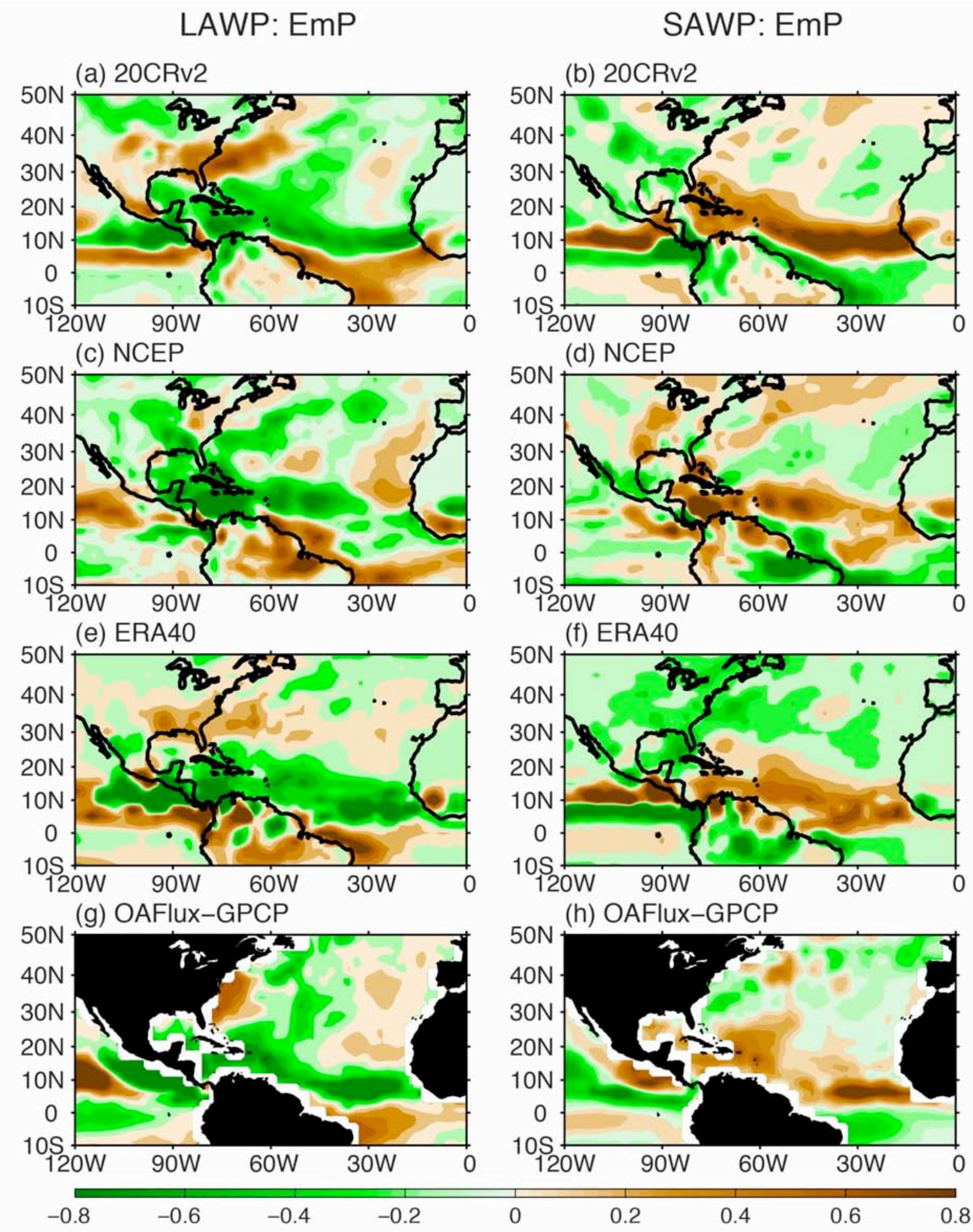

Figure 7. Composites of the EmP anomalies (mm/day) on interannual timescales during the summer (JJA). Shown are for large AWP (left panels) and small AWP (right panels) from various data sets of (a, b) 20CRv2, (c, d) NCEP, (e, f) ERA40 and (g, h) OAFlux-GPCP.

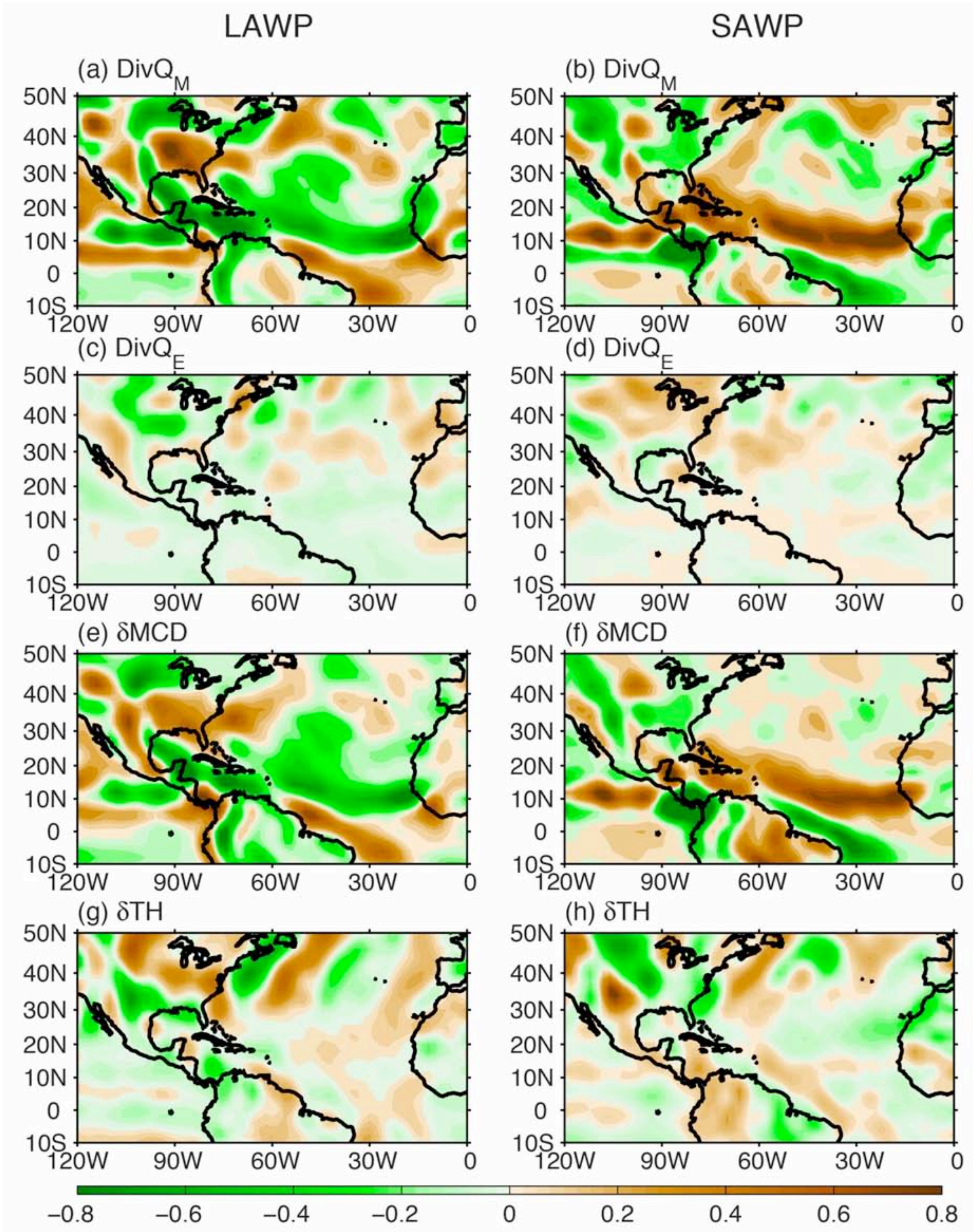

Figure 8. Composites of the moisture flux divergence anomalies on interannual timescales for large AWP (left panels) and small AWP (right panels) during the summer (JJA). Shown are the moisture flux divergence from (a, b) monthly to longer timescales of $DivQ_M$ and from (c, d) the transient eddies of $DivQ_E$. $DivQ_M$ is further decomposed into (e, f) the mean circulation dynamics contribution of δMCD and (g, h) the thermodynamics contribution of δTH. Unit is mm/day. The composites are calculated based on 20CRv2.

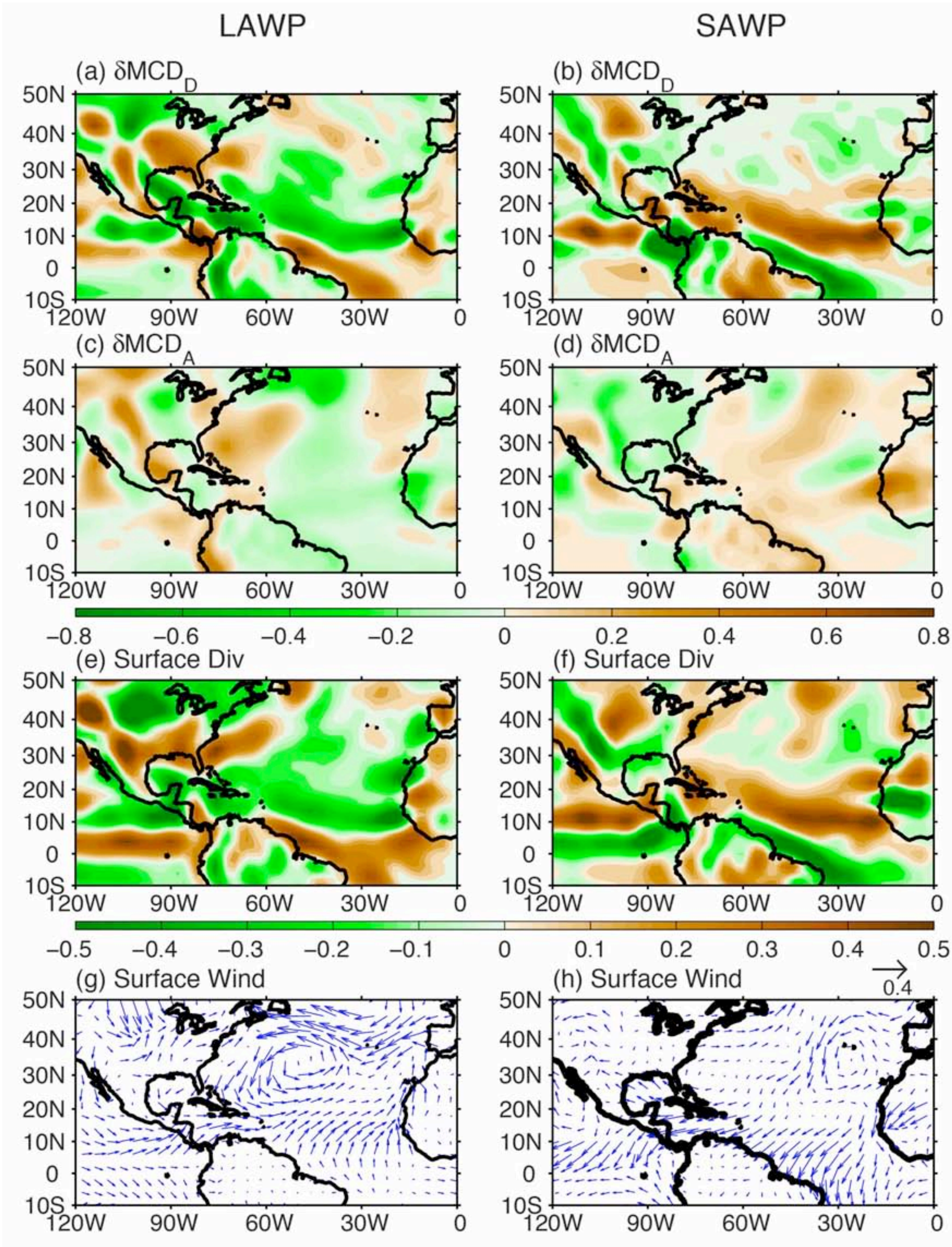

Figure 9. Composites of the moisture change (mm/day) due to mean circulation dynamics on interannual timescales for large AWP (left panels) and small AWP (right panels) during the summer (JJA). Shown are the contribution by (a, b) the wind divergent change and (c, d) the advection of moisture by the wind change. Composites of the 925-hPa wind divergence and wind anomalies are shown in (e, f) and (g, h), respectively. The composites are calculated based on 20CRv2.

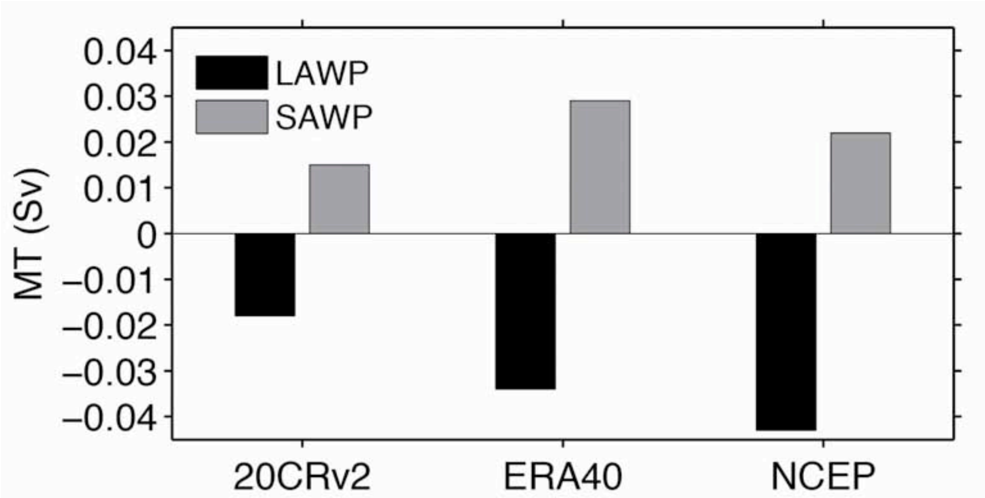

Figure 10. Composites of the cross-Central America moisture transport anomalies on interannual timescales for large AWP and small AWP during the summer (JJA) using the data sets of 20CRv2, NCEP and ERA40.

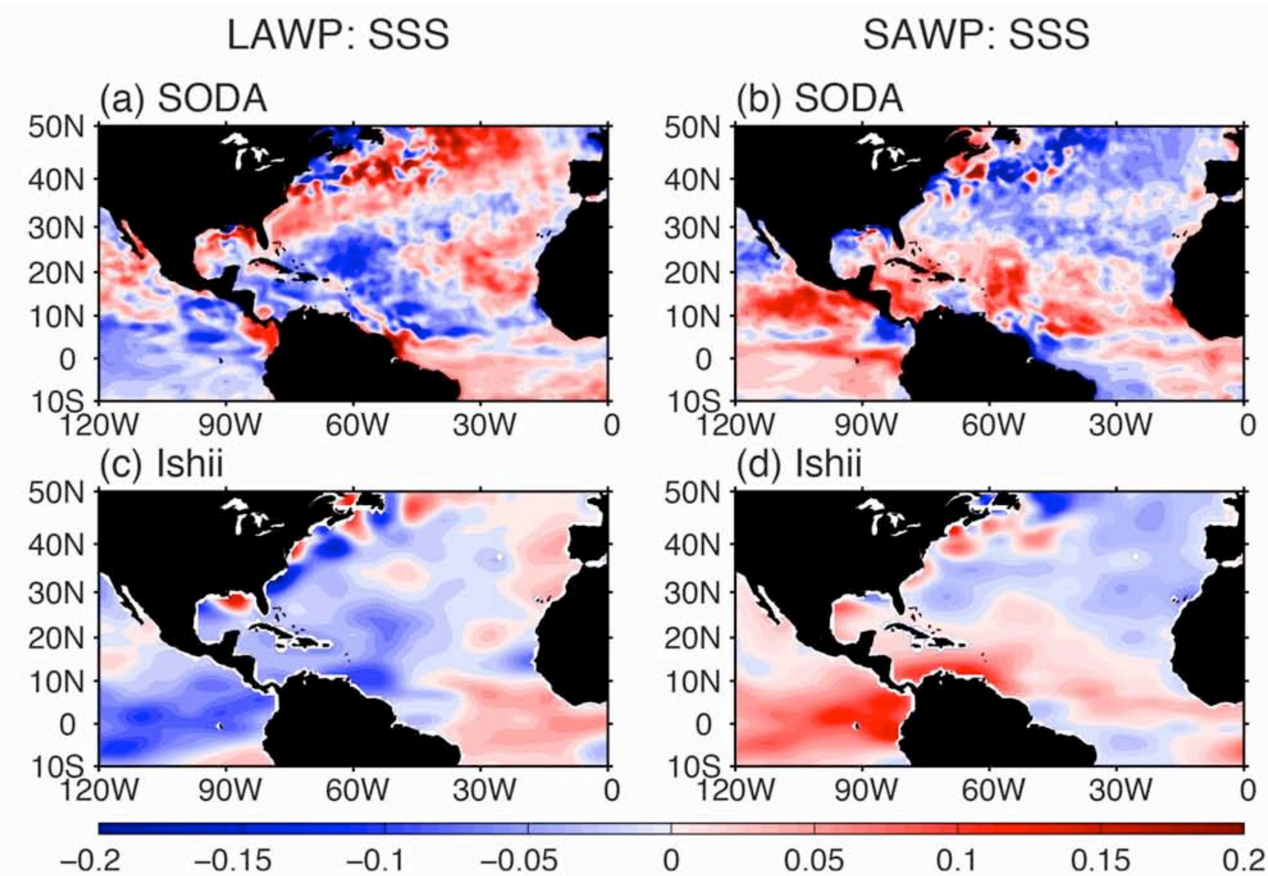

Figure 11. Composites of the sea surface salinity (SSS) anomalies (psu) on interannual timescales for large AWP and small AWP during the summer (JJA) based on the SODA and Ishii data.

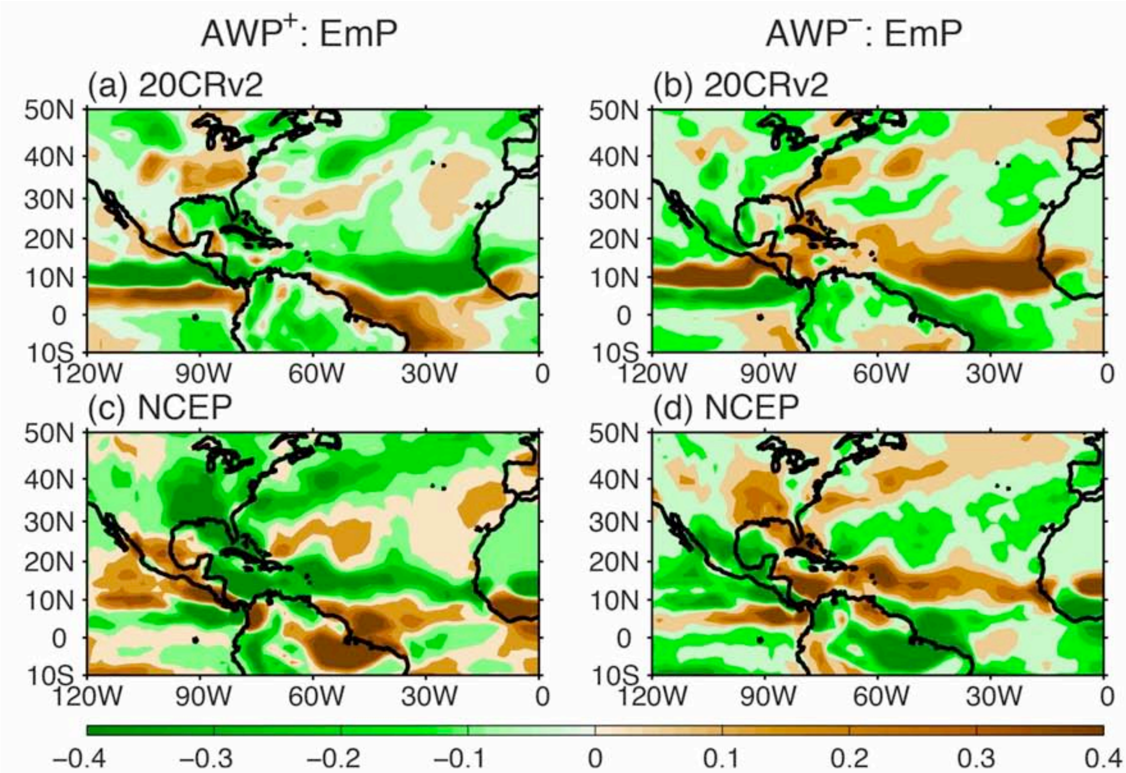

Figure 12. Composites of the EmP anomalies (mm/day) on multidecadal timescales during the summer (JJA). Shown are for the positive phase of the AWP (left panels) and the negative phase of the AWP (right panels) from the data sets of (a, b) 20CRv2 and (c, d) NCEP.

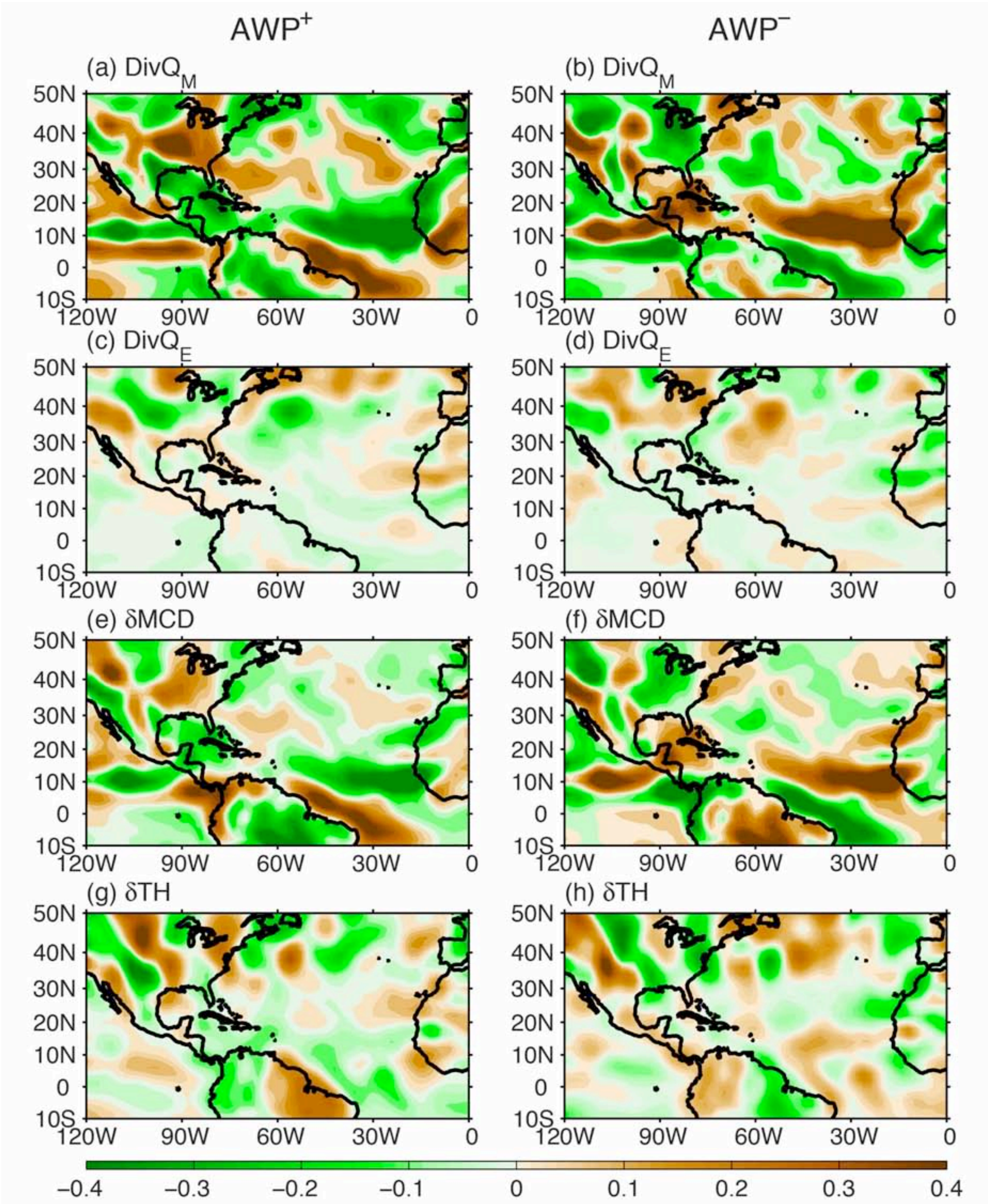

Figure 13. Composites of the moisture flux divergence anomalies on multidecadal timescales during the summer (JJA) for the positive phase of the AWP (left panels) and the negative phase of the AWP (right panels). Shown are the moisture flux divergence from (a, b) monthly to longer timescales of $DivQ_M$ and from (c, d) the transient eddies of $DivQ_E$. $DivQ_M$ is further decomposed into (e, f) the mean circulation dynamics contribution of δMCD and (g, h) the thermodynamics contribution of δTH. Unit is mm/day. The composites are calculated based on 20CRv2.

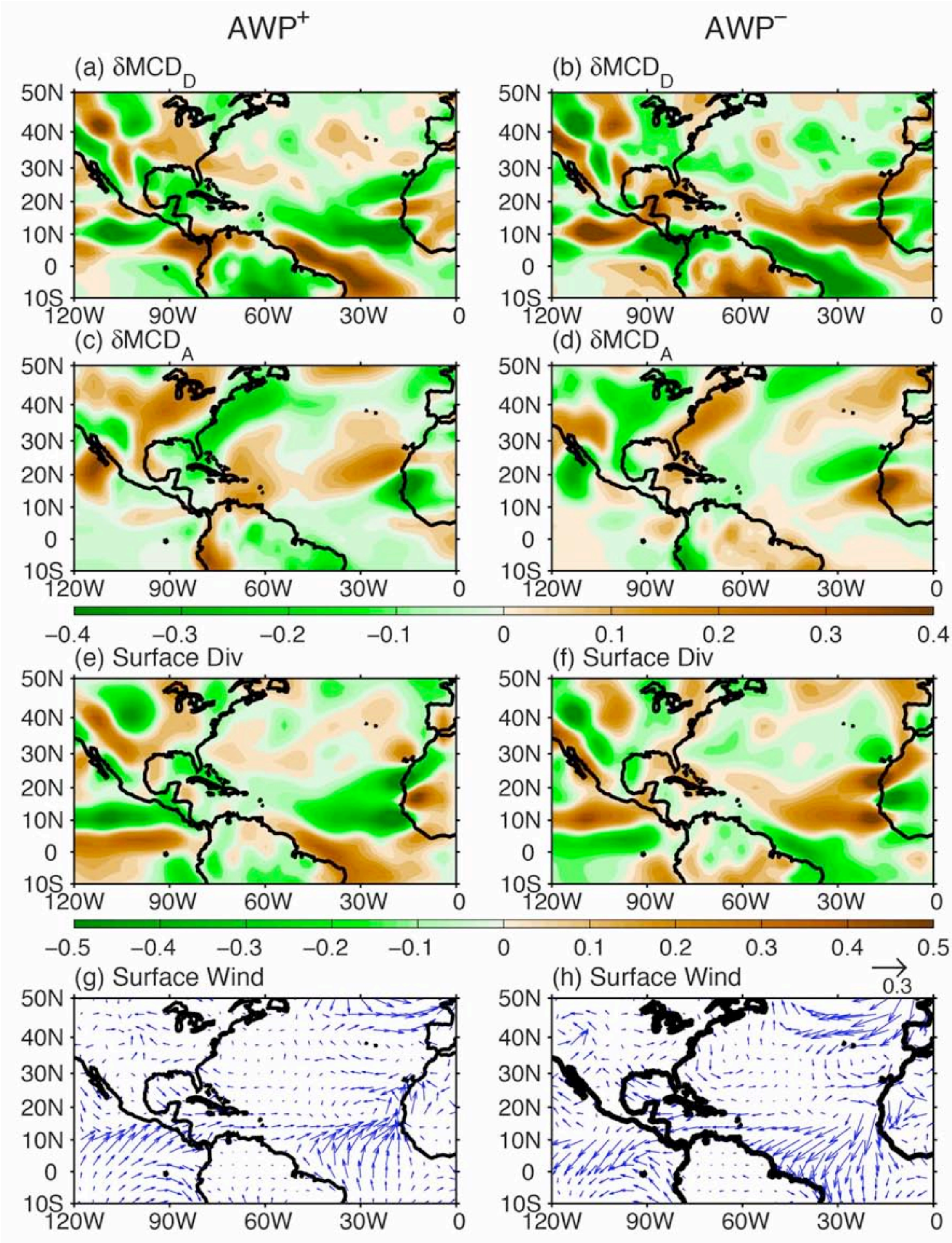

Figure 14. Composites of the moisture change (mm/day) due to the mean circulation dynamics on multidecadal timescales during the summer (JJA) for the positive phase of the AWP (left panels) and the negative phase of the AWP (right panels). Shown are the contribution by (a, b) the wind divergent change and (c, d) the advection of moisture by the wind change. Composites of the 925-hPa wind divergence and wind anomalies are shown in (e, f) and (g, h), respectively. The composites are calculated based on 20CRv2.

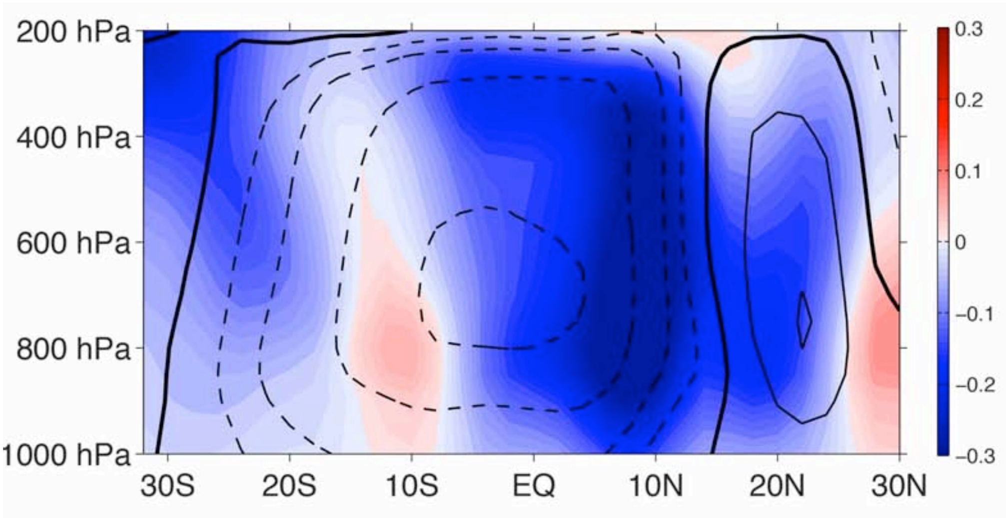

Figure 15. The Hadley circulation during the summer (JJA) defined as the zonal mean stream function in 20CRv2. The contour lines represent the climatological Hadley cell and the shading denotes the difference of the Hadley cell between the positive and negative phases of the AWP on multidecadal timescales. Contour interval is 20×10^{9} kg s^{-1}.

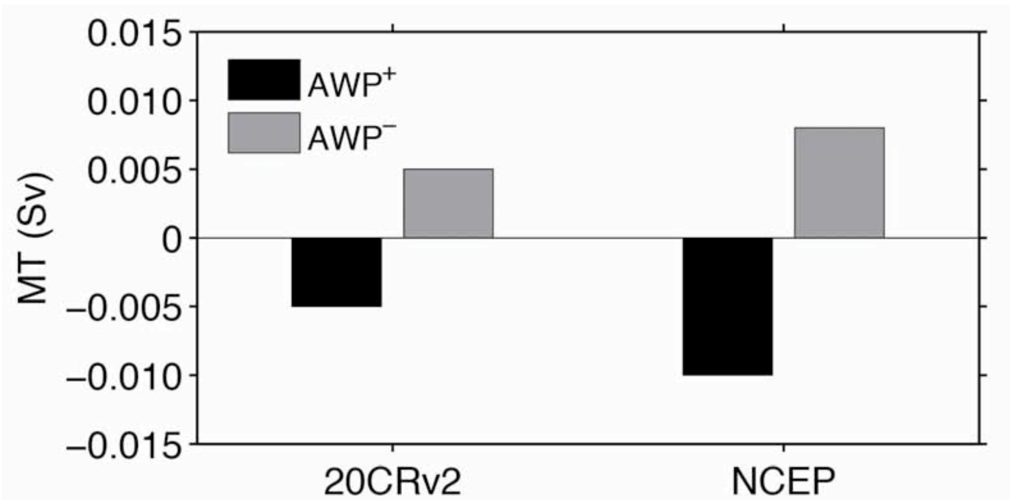

Figure 16. Composites of the cross-Central America moisture transport anomalies (Sv) on multidecadal timescales during the summer (JJA) for the positive and negative phases of the AWP using the data sets of 20CRv2 and NCEP.

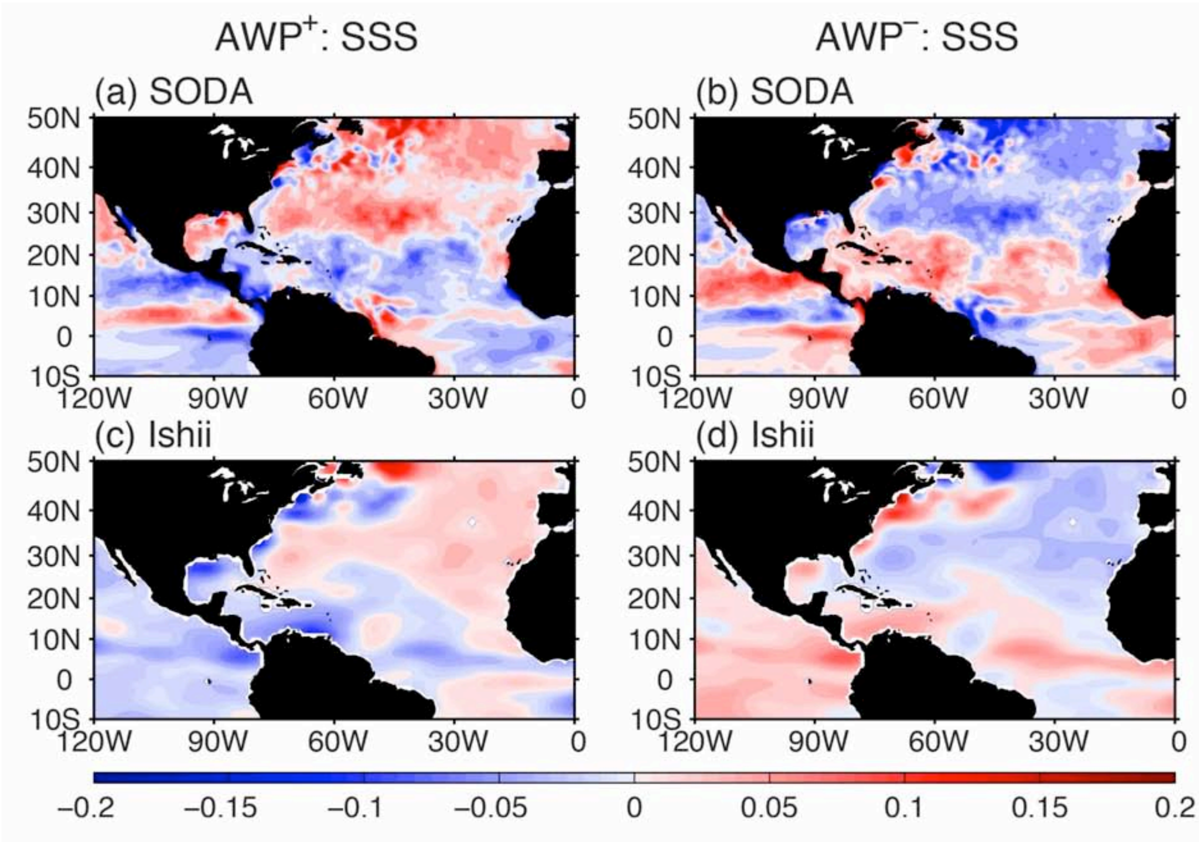

Figure 17. Composites of the sea surface salinity (SSS) anomalies (psu) on multidecadal timescales during the summer (JJA) for the positive phase of the AWP (left panels) and the negative phase of the AWP (right panels) based on the SODA and Ishii data.